



1 Rift and plume: a discussion on active and passive rifting 2 mechanisms in the Afro-Arabian rift based on synthesis of 3 geophysical data

4 Ran Issachar^{1,2}, Peter Haas¹, Nico Augustin³ and Jörg Ebbing¹

5 ¹Institute for Geosciences, Kiel University, Geophysics, Kiel, Deutschland, ²Geological Survey of Israel, Jerusalem, Israel,

6 ³GEOMAR Helmholtz Centre for Ocean Research, Dynamics of the Ocean Floor, Kiel, Deutschland

7 *Correspondence to:* Ran Issachar (ranis@gsi.gov.il)

8 Abstract

9 The causal relationship between the activity of mantle plumes and continental break-up is still elusive. The
10 Afro-Arabian rift system offers an opportunity to examine these relationship, in which an ongoing
11 continental break-up intersects a large Cenozoic plume related flood basalt series. In the Afar region, the
12 Gulf of Aden, the Red-Sea and the Main Ethiopian Rift form an R-R-R triple junction and separate the
13 Ethiopian and Yemen Traps by ~600 km. We provide an up-to-date synthesis of the available geophysical
14 and geological data from this region. We map the rift architecture in the intersection region of the rifts
15 and review the spatio-temporal constraints in the development of the different features of the plume-rift
16 system.

17 We infer two spatial constraints in the development of the rifts: (1) the connection of the Main Ethiopian
18 Rift to the Gulf of Aden and to the Red Sea by its northeastward propagation; (2) the abandonment of an
19 early tectonic connection between the Red Sea and the Gulf of Aden. Additionally, chronological evidence
20 suggests that regional uplift and flood basalt eruptions sufficiently preceded rifting. By this, we infer a
21 progressive development in which the onset of the triple junction marks a tectonic reorganization and was
22 the last feature to develop, after all rift arms were thoroughly developed. We argue that the classical active
23 and passive rifting mechanisms cannot simply explain the progressive development of the Afro-Arabian
24 rift and propose a scenario of plume-induced plate rotation that includes an interaction between active
25 and passive mechanisms. In this scenario, the arrival of the Afar plume provided a push-force that
26 promoted the rotation of Arabia around a nearby pole, enabling rifting and ultimately the break-up of
27 Arabia from Africa.

28

29 Short summary:

30 We explore the causal relationship between the arrival of the Afar plume and the initiation of the Afro-
31 Arabian rift. We mapped the rift architecture in the triple junction region from geophysical data and
32 reviewed the available geological temporal evidence. We infer a progressive development of the plume-
33 rift system and suggest an interaction between active and passive mechanisms in which the plume
34 provided a push-force that changed the kinematics of the associated plates.



35 1. Introduction

36 The causal dependency between the eruption of flood basalts and continental break-up is still unclear,
37 although a close occurrence between these two phenomena has been recognized for a long time.
38 Continental flood basalts, often referred to as traps, form large igneous provinces covering huge
39 continental areas (Bryan and Ferrari, 2013; Ernst, 2014). They are associated with extensive volcanism
40 during short time intervals, brought to the surface by deep-seated mantle plumes (Richards et al., 1989;
41 White and McKenzie, 1995; Koppers et al., 2021). Observations indicate a close temporal and spatial
42 occurrence between the eruption of flood basalts and continental break-up. In particular, when
43 reconstructed back to their original plate tectonic configuration, a R-R-R triple junction is found within the
44 flood basalts areas (Morgan, 1971; Burke and Dewey, 1973; Buitert and Torsvik, 2014). Using the geological
45 record to examine the mutual dependency of these processes is challenging. It requires high-precision
46 constraints regarding the temporal and spatial development of the different volcanic and tectonic
47 features, often obscured by the long geological history.

48 The Afar region in the central parts of the Afro-Arabian rift system is recognized as a key locality to examine
49 models of plume-rift association, offering a young and active case study in which plume, regional uplift, R-
50 R-R triple junction, break-up, and oceanic spreading co-exist and are superimposed (Fig. 1). Plume-rift
51 association is mainly explained by either ‘active’ (e.g., Sengör and Burke, 1978) or ‘passive’ (e.g., White
52 and McKenzie, 1989) views, with no interaction between those modes, although some evidence suggest
53 more complex effect of plumes on the regional plate kinematics (e.g., Cande and Stegman, 2011). Despite
54 the contrary implications of the ‘active’ and ‘passive’ views, the Afar case study was used as a prime
55 example to support both, and some authors argued that both processes are required to explain the
56 observations (Burke and Dewey, 1973; White and McKenzie, 1989; Courtillot et al., 1999). The discrepancy
57 can be primarily attributed to a lack of accurate geological and geophysical evidence, leading to contrary
58 interpretations.

59 The purpose of this paper is to utilize a synthesis of the available geological and geophysical data from the
60 Afar region and to use it for geodynamic implications in the study area. We first review the evidence
61 regarding the temporal association of the volcanic and rift components of the system. This review is
62 essential because large amounts of new data were collected in recent years, enabling a re-examination of
63 the relationships between the plume and the rifting. We further provide an analysis and interpretation of
64 modern geophysical datasets, including topography, bathymetry, gravity, magnetic anomalies,
65 earthquakes and volcano distribution. Using these datasets we map the architecture of the rift margins
66 and axes and infer spatial constraints in the development of the rift segments. Finally, we discuss the
67 results in the light of recent models and from other case studies in the world, aiming to shed light on the
68 causal relationship between mantle plumes and tectonic processes in the crust.

69 2. Active and passive mechanisms for plume-rift association

70 The existence of deep mantle convection and its interaction with the Earth’s crust was already pointed out
71 by Wilson (1963), and a close occurrence to continental break-up was soon noticed by the abundance of
72 hotspots near many rift junctions (Morgan, 1971) and flood basalts volcanism along passive margins
73 (Richards et al., 1989). This led Morgan (1971) to speculate that deep mantle convection has a significant
74 role in accelerating the overlying tectonic plates. Nevertheless, it was later realized that slab-pull provides



75 the main driving force for plate motion. Furthermore, plumes are thought to have a major role in plate
76 tectonics, triggering rifting by weakening the upper lithosphere. In their landmark paper, Burke and Dewey
77 (1973) presented 45 case studies of rift junctions associated with hot spots. They proposed a model in
78 which plume-associated uplift and volcanism precede and generate rifts, initiated from a triple junction
79 within the plume region. Afar was used as a first and prime example, highlighting its importance as a young
80 and active case study; however, they already noted its complexity (Burke and Dewey, 1973).

81 Following these insights, ‘active’ rifting models were developed to explain plume-rift associations (e.g.,
82 Keen, 1985; Moretti and Froidevaux, 1986; Campbell and Griffiths, 1990; Hill, 1991; White and McKenzie,
83 1995). These models generally propose that rifting can result from a combination of processes derived by
84 the actively rising head of anomalously hot mantle. These include impinging and eroding the base of the
85 lithosphere, which prompt uplift and decompression melting, which in turn introduces internal extensional
86 forces and ultimately leads to break-up. Accordingly, in this view, regional uplift and volcanism are
87 expected to precede rifting, which would initiate from a triple junction above the mantle plume head (Fig.
88 2a).

89 Later contributions challenged the active view, arguing that a ‘passive’ asthenospheric upwelling can also
90 resolve the occurrence of flood basalt near rifts (firstly introduced by White and McKenzie, 1989). In this
91 view, rifting is initiated by the remote stresses, usually along former sutures and weak zones, regardless
92 of underlying plumes. The production of massive volcanism is allowed when the thinned and stretched
93 lithosphere is underlain by a thermal anomaly in the mantle. The volcanism is generated by decompression
94 melting of hot asthenospheric mantle, passively rising. As plumes form large areas of higher temperatures
95 in the mantle, massive volcanism is found on earth’s crust close to rifts. Accordingly, in this view,
96 subsidence is a precondition required for magmatism, and there is no particular reason for a triple junction
97 to form within the flood basalts region (Fig. 2b).

98 Although active and passive views have been discussed in the last 50 years, the role of plumes in initiating
99 rifting is still unclear and much debated. Even for well-studied and prime examples of plume-rift
100 association as the Siberian, Parana-Etendeka, Deccan and Greenland traps there is no agreement whether
101 active processes initiated rifting (Geoffroy, 2005; Ivanov et al., 2015; Frizon De Lamotte et al., 2015; Fromm
102 et al., 2015; Mitra et al., 2017). Some authors emphasize the significance of preexisting lithosphere
103 weaknesses along structural inheritance and former sutures (Buiter and Torsvik, 2014; Will and Frimmel,
104 2018), while others show the potential of plumes to thermally and chemically erode the base of the
105 lithosphere in the weakening process allowing rifting (Sobolev et al., 2011). Additionally, some models
106 demonstrate that mixed active-passive scenarios can better explain observation (Koptev et al., 2018), and
107 even that both mechanisms are needed to explain temporal variations in rifts (Huismans et al., 2001).

108 In addition to the dichotomic views, some evidence imply more complex relationships between plumes
109 and the kinematics of the associated plates (van Hinsbergen et al., 2011; Cande and Stegman, 2011;
110 Chatterjee et al., 2013; Pusok and Stegman, 2020). These studies discuss the role of plumes in changing
111 the relative motions of the overlying plates and suggest that lateral forces, induced by the arrival of the
112 plume head, can add up to the remote stresses, change the plate kinematics and even trigger the
113 formation of new plate boundaries (van Hinsbergen et al., 2021) (Fig. 2c). Thus, in this view the plume is
114 changing the remote stress field, which in-turn allows rifting.



115 3. Geological setting

116 The Afro-Arabian rift system is extending from Turkey to Mozambique (McConnell and Baker, 1970) and
117 is the current episode of the Phanerozoic break-up of the East African continental plate (Bosworth, 2015).
118 It contains the rifting in the Gulf of Aden, in the Red Sea and in East Africa. In the center of that system,
119 the Ethiopian northwestern and southeastern plateaus represent an elevated topography with a highest
120 peak of 4,620 m (Ras Dashan) and an average elevation of 2000 m above sea level. This area is part of the
121 so-called African Superswell, a wide region of anomalously high topography comprising East Africa
122 (Lithgow-Bertelloni and Silver, 1998; Corti, 2009). In western Yemen, the Sarawat Mountains are the
123 highest peaks in the Arabian Peninsula, reaching more than 3,000 m, at only 100 km from the shoreline of
124 the Red Sea. The mountains show a typical stair morphology with steep slopes at the western and southern
125 sides, while the eastern side of the mountains slopes downward more gently.

126 The Gulf of Aden is the most developed rift segment in the Afro-Arabian rift, with a mature and fully
127 developed oceanic spreading center connected to the mid-ocean ridge in the Indian Ocean. Six pairs of
128 magnetic stripes are recognized along the Gulf of Aden ridge (Fournier et al., 2010) (Fig. 3). Oblique rifting
129 and high angle structural inheritance along the Gulf of Aden resulted in multiple ridge segments and
130 fracture zones (i.e., transform faults; Leroy et al., 2013; Autin et al., 2013; Bellahsen et al., 2013; Duclaux
131 et al., 2020).

132 At the northern parts, rifting in the Red Sea is connected by the Dead Sea Fault to the Eurasian collision
133 zone along the Taurus-Zagros Mountains. The Red Sea is currently experiencing the last stages of break-
134 up and early stages of oceanic accretion. An oceanic spreading center with three pairs of ridge parallel
135 magnetic stripes is developed in the southern parts of the Red Sea (Schettino et al., 2016) (Fig. 3). However,
136 oceanic crust is probably flooring most of the basin (Augustin et al., 2021).

137 The Main Ethiopian Rift is the northernmost section of the intra-continental rifting in East Africa, splitting
138 the not yet well individualized Somali plate from Africa (Chorowicz, 2005). Current rifting in the Main
139 Ethiopian Rift is characterized by a narrow rift valley, in which volcanic and tectonic activities are localized
140 and influenced by oblique rifting conditions (Corti, 2009).

141 The Afar triangle is the region where the above mentioned three rift arms meet (Fig. 3). It is considered as
142 a geological depression as it is an area of low elevation compared to the high Ethiopian plateaus, and thus
143 commonly referred to as the Afar 'depression'. Nevertheless, this term is misleading as the Afar triangle is
144 included within the rifted area and is geologically elevated from the deep bathymetry of the Gulf of Aden
145 and the Red Sea basins. The Afar triangle is mainly floored by Pliocene and younger volcanic rocks, where
146 Miocene volcanic series are exposed along the western margins and at the elevated Danakil block. It
147 comprises many volcanoes that compose axial volcanic ranges (Fig. 2), where the Red Sea side is
148 characterized by transverse volcanic fields and the southern side by central volcanoes (Varet, 2018). Two
149 magnetic isochrons have been recognized in the Tendaho graben, indicating young oceanization in central
150 Afar (Bridges et al., 2012). Structurally, several mega-scale accommodation zones connecting the different
151 rift segments and a triple junction location is recognized at 11.0°N, 41.6°E at the Tendaho-Goba'ad
152 Discontinuity (e.g. Tesfaye et al., 2003) (Fig. 3).



153 4. Temporal constraints

154 4.1. Flood basalts and uplift

155 Vast efforts were made to study the chemistry and chronology of flood basalts in East Africa (see review
156 by Rooney, 2017). Two phases of extensive flood basalt volcanism are associated with plume-lithosphere
157 interaction (Fig. 4). The early phase is mainly confined to southern Ethiopia and northern Kenya. The timing
158 of this event is poorly constrained to 45-35 Ma (George et al., 1998). The second phase of flood basalt
159 eruptions was more voluminous, more widespread and shorter-lived. Earliest basalts of this phase date
160 back to 34 Ma near Tana Basin, Ethiopia (Prave et al., 2016) and 31 Ma in western Yemen (Peate et al.,
161 2005) (Fig. 4). The traps accumulated very rapidly, in less than 6 Ma (Coulié et al., 2003), and include
162 tholeiitic to alkaline compositions of asthenosphere mantle source (Mattash et al., 2013). Thick sequences
163 of up to 2 km are observed within a widespread region in Ethiopia and Kenya (Bellieni et al., 1981; Wescott
164 et al., 1999; McDougall and Brown, 2009). It is commonly accepted that these flood basalts are of a deep
165 seated mantle plume origin (Koppers et al., 2021). However, the mechanism is debatable and may involve
166 multiple plume impingements within a broad upwelling zone connected to the African superplume in the
167 lower mantle (Meshesha and Shinjo, 2008) or a single plume–lithosphere interaction (Rooney, 2017).

168 An elevated topography is associated with the eruption of the flood basalts in Ethiopia. The flood basalts
169 are almost exclusively positioned within the elevated regions of the Ethiopian and Somalian plateaus and
170 the Sarawat Mountains in southwest Yemen (Fig. 1). Dynamic topography component supports up to 1 km
171 of present-day elevation of the Ethiopian and Somalian plateaus, confirming the significant contribution
172 of mantle convection to the regional uplift (Gvirtzman et al., 2016). Although the uplift chronology is not
173 easily resolved, recent studies infer it is a long-term feature, already present before the emplacement of
174 the flood basalts (Sembroni et al., 2016; Faccenna et al., 2019). Regional uplift is estimated to begin before
175 40 Ma, with maximal uplifts between 12 and 28 Ma, reaching an average elevation of 2500 m (Fig. 4)
176 (Sembroni et al., 2016).

177 4.2. Gulf of Aden

178 The beginning of continental rifting in the Gulf of Aden is only approximately known (Bosworth et al.,
179 2005). Estimates mainly rely on the dating of sedimentary sequences, and no recent data was published.
180 The evidence of rift initiation was summarized by Bosworth et al. (2005). Various sedimentary indications,
181 including onshore outcrops in Yemen (Watchorn et al., 1998) and in Oman (Roger et al., 1989) and offshore
182 wells (Hughes et al., 1991), suggest that rifting in the central and eastern Gulf of Aden began at early to
183 mid-Oligocene, within the Rupelian, i.e., 33.9 - 27.8 Ma. Syn-rift sediments from the central Yemeni
184 margins indicate that rift flank uplift occurred before any significant regional extension. Continental rifting
185 climax is estimated between 20 and 18 Ma (Watchorn et al., 1998). Radiometric dating indicates that the
186 margins became stable already in the Early Miocene (Bosworth et al., 2005), and rift-to-drift transition is
187 interpreted to occur between ~21.1 and ~17.4 Ma (Watchorn et al., 1998). The seafloor spreading center
188 in the Gulf of Aden is developed along most of its length and is connected to the mid-ocean ridge in the
189 Indian ocean through the Sheba Ridge (Gillard et al., 2021). In the central Gulf of Aden, magnetic isochrons
190 suggest opening rates of ~27 mm/yr prior to 11 Ma, and a slowdown after 11 Ma (Fig. 4). Chron 5C (purple
191 stripes in Fig. 3; 16.0 Ma) is present along the Gulf of Aden up to the Shukra al Sheik discontinuity (Fournier
192 et al., 2010). This implies that the spreading center developed very rapidly, perhaps instantaneously in
193 geological time scales, covering a distance of more than 700 km in less than 1.5 Ma. This fast propagation



194 ceased at the Shukra al Sheik discontinuity (Fig. 3). The youngest magnetic isochrons (2A, 2.6 Ma) is
195 recognized up to longitude 43.9°E in the eastern Gulf of Tadjoura, ~150 km west to the Shukra al Sheik
196 discontinuity, indicating that along this segment, the ridge propagated westward at an average rate of ~11
197 mm/yr, in the last 16 Ma. Within the Gulf of Tadjoura, no direct evidence of oceanic spreading was
198 reported to our best knowledge.

199 4.3. Red Sea

200 It is not certain when continental rifting in the Red Sea began; however, sedimentary sequences suggest
201 it postdates rifting in the Gulf of Aden by a few million years (Bosworth et al., 2005). Independent evidence
202 suggests that rifting had begun simultaneously along the entire Red Sea at late Oligocene–Early Miocene,
203 ~23 Ma (Plaziat et al., 1998; Szymanski et al., 2016; Stockli and Bosworth, 2018; Morag et al., 2019).
204 Magnetic isochrons associated with seafloor spreading are only known from the southern parts of the Red
205 Sea. However, oceanic lithosphere is probably abundant along most of the basin (Augustin et al., 2021).
206 Chron 3 (4.2 Ma) is only present between latitudes 16° and 18°, while chrons 2A (2.6 Ma) and 2 (1.8 Ma)
207 are present up to latitude 22° (Schettino et al., 2016). Structural reconstructions, geodetic measurements,
208 and magnetic stripes suggest opening rates of ~11 mm/yr in the central parts of the basin, with an abrupt
209 increase at ~5 Ma (Fig. 4) (Schettino et al., 2018). The southern edges of the magnetic chrons suggest that
210 the ridge rapidly propagated southwards, with rates of ~30 mm/yr, between chrons 3 (4.2 Ma) and 2A (2.6
211 Ma). However, the rapid propagation was halted in the last 2.6 Ma (Fig. 3).

212 4.4. Main Ethiopian Rift

213 Results from many years of extensive fieldwork (see Corti, 2009 for review) suggest a diachronous
214 development of the different segments of the Main Ethiopian Rift. However, there is no agreement
215 regarding the exact timing of events and even regarding the propagation trend of the rift. Reconstructions
216 based on magnetic anomalies from the Southwest Indian ridge suggest an upper limit for the Nubia-
217 Somalia separation at ~19 Ma, including large uncertainties (DeMets and Merkuriev, 2016) (Fig. 4). There
218 are indications that rifting in East Africa started at the Turkana depression in southern Ethiopia (Varet,
219 2018) and propagated north to Afar (Wolfenden et al., 2004); however, this is still a matter of debate (see
220 figs 42-44 in Corti, 2009). Radiometric dating of structural features indicates that extension commenced
221 at ~11 Ma within the northern Main Ethiopian Rift (Wolfenden et al., 2004).

222 In summary, regional uplift and flood basalt volcanism in Ethiopia preceded rifting of the Afro-Arabian rift.
223 The rift arms developed at different times, when rifting in the eastern Gulf of Aden started during last
224 phases of flood basalt volcanism in Ethiopia. Rifting in the Red Sea and in the Main Ethiopian Rift started
225 in a lag of ~5-7 Ma after flood basalt volcanism.

226 5. Data and Methods

227 We used bathymetry and topography data to identify morphotectonic features. To highlight and map the
228 architecture of the margins and axes of the rifts we applied the Difference of Gaussians method to the
229 topography and the bathymetry grids (Akram et al., 2017). This method allows a fast and accurate edge
230 detection of elevation using active spatial bandpass filtering. We applied luminance coloring to the
231 resulted grid using the open-source image processing software, Gimp.org.



232 To study density-related shallow crustal structures, we used the satellite altimetry-derived vertical gravity
233 gradient (VGG) model of Sandwell et al., (2014), offering 1 arc-min resolution at offshore regions. As higher
234 frequencies are intensified in the spectral power of the VGG, its anomalies are more source-localized and
235 shallow-sensitive than free-air anomalies. To enhance the edges associated with the VGG, we applied a
236 linear 11-colors colormap, further applied transparency to the VGG map, and projected it on a shaded
237 relief (Fig. 5a).

238 To study deeper crustal structures and eliminate topography effect, we used Bouguer gravity anomaly
239 (BGA), derived from the XGM2019 gravity model (Zingerle et al., 2020), calculated with a grid step of 0.1
240 degrees. The XGM2019 is the most updated global gravity model of the ICGEM and is provided in terms of
241 spherical harmonics up to 2159 degree (Ince et al., 2019; Zingerle et al., 2020). In addition, we applied a
242 linear 240-colors colormap to enhance BGA structures, further applied transparency to the BGA map, and
243 projected it on a shaded relief (Fig. 5b).

244 To better correlate and discriminate crustal structures and rift features, we considered 1913 earthquake
245 locations from the International Seismological Centre catalogue with minimum magnitudes above 4 ML,
246 recorded between 1964 and 2019. To better infer recent tectonic and volcanic activity, we further
247 considered the locations of Quaternary onshore volcanoes, from the Global Volcanism Program
248 (Smithsonian Institution) and from google earth mapping.

249 6. Results

250 6.1. Rift margins

251 The most prominent morphological feature of the rift system is the sharp cliff along its shoulders. The
252 shoulder cliffs mark the rift margin as they distinguish between (1) uplifted pre-rift rocks of the Arabo-
253 Nubian shield or trap basalts sequences and (2) Quaternary arid fluvial sediments or young volcanic
254 sequences. Thus, the shoulder cliffs have a very distinctive appearance in the topographical and gravity
255 data. The edge detection analysis of topography and bathymetry data allows us to outline the rift margins
256 (Fig. 6).

257 In the Red Sea, the shoulder cliffs are generally continuous with an average rift width of 440 ± 20 km
258 (calculated perpendicular to the Red Sea axis in the study area), and a general increase in rift width from
259 north to south (Fig. 6b). We identify two segments that mark an abrupt change in rift orientation and rift
260 width: (1) Below latitudes 15.5° on the African margin and 18° on the Arabian margin (segment I in Fig. 6),
261 the rift shoulders deviate from their general parallel to the Red Sea trend, bending towards the Afar region.
262 The cliff is characterized by seismic activity from that point on the African side, which is also considered
263 the northern point of the western Afar margins (Zwaan et al., 2020). (2) Below latitudes 12.5° on the
264 African margin and 15° on the Arabian margin (segment II in Fig. 6), we identify another abrupt change,
265 both in the orientation and the width of the rift. That point on the African margin is the intersection of the
266 Tendaho-Goba'ad Discontinuity with the Western Afar Margins (Tsfaye et al., 2003). We note that these
267 changes are noticeable and similar both on the African and the Arabian sides.

268 In the Gulf of Aden, the shoulder cliffs generally follow the trend of the basin. In the western parts the
269 shoulder cliffs are less straight and less continuous than those of the Red Sea and generally reflect the
270 sinistral basin structures. This morphology is well explained by oblique rifting along the Gulf of Aden (Leroy



271 et al., 2013). The average rift width in the study area is 470 ± 45 km (calculated rift-perpendicular), with a
272 general eastward increase (Fig. 6b). We recognize an abrupt change in rift width along three lines (III-V in
273 Fig. 6), which are associated with fracture zones. Along the Somalian margin prominent sinistral offsets
274 are recognized along lines III and V. This cliff segment is a morphological continuation of the Tendaho-
275 Goba'ad Discontinuity lineament, and is also prominent in the VGG map (Fig. 5a).

276 Although recognizable in the processed topography map, the rift shoulders are less sharp in the Main
277 Ethiopian Rift (Fig. 6a). They are prominent in the gravity data as they are associated with VGG and BGA
278 highs (see profile A in Fig. 9). In the Afar region, the margins show a funnel shape (Fig. 6a). The distance
279 between the Somalian and Ethiopian escarpment is steadily and monotonically increasing from the Main
280 Ethiopian Rift to the Tendaho-Goba'ad Discontinuity (Fig. 6b), suggesting that this segment is intact and
281 non-disturbed by the other arms of the rift system.

282 In summary, the rift margins of the Red Sea and the Gulf of Aden are interrupted with the proximity to the
283 Afar region, whereas the margins of the Main Ethiopian Rift smoothly funnel into the Afar region.

284 *6.2. Rift axes*

285 Along the Red Sea and the Gulf of Aden basins, the rift axes are distinctively characterized by deep and
286 sharp bathymetric troughs, VGG lows, BGA highs, and intense seismic activity. However, with the proximity
287 to the Afar region, the rift axes change their characteristics.

288 The rift axis along the Red Sea is outlined by a deep and wide axial trough that ends at latitude 14.5° ,
289 approximately 400 km from the triple junction (Fig. 7a). South of latitude 14.5° , we find geophysical
290 evidence that the rift axis is bent, entering the Afar region at the Bay of Beylul (latitude 13.3°): (1) The VGG
291 signature of the Red Sea axis, with highs along the walls of the axial trough and a low above the center
292 (Fig. 7b and profile B). (2) A trail of volcanic islands follows its path (Hanish-Zukur Islands; Fig. 3). (3) A
293 general trend of recent onshore magmatism meets this line at the Bay of Beylul (Fig. 3). (4) This line also
294 best fits GPS based rigid block model (Viltres et al., 2020). In addition to this segment, a typical gravity
295 signature of the rift axis with a central BGA high and VGG picks to its side, is also recognized along the
296 connection of the Red Sea with the Gulf of Aden at Bab al Mandab Strait (latitudes 13.2° to 12.3° ; Fig. 7
297 profile CC'). Nevertheless, this segment is not an active rift axis as no earthquake, volcanic or bathymetrical
298 expression is associated with it (Fig. 3).

299 In the Gulf of Aden, there is also a distinct change in the rift axis characteristics, approximately 400 km
300 from the triple junction (Fig. 8). Up to the Shukra al Sheik discontinuity, the Gulf of Aden is a deep basin,
301 reaching depths of more than 1,000 m only a few kilometers from the shore, and has a fragmented axial
302 trough, offset by oblique left-lateral transform faults. West to the Shukra al Sheik discontinuity, the basin
303 is shallow, and the axial trough is very distinct, characterized by deep and sharp morphology. This ~400
304 km long curved segment of the axis impales the Afar triangle at the Gulf of Tadjoura (Djibouti). This axial
305 segment has a distinct gravity signature and is characterized by intensive seismic activity, perhaps the most
306 intensive in the rift system, with over 1000 recorded events with magnitude above 4ML (ISC catalogue).

307 In the Main Ethiopian Rift, there are no abrupt changes in the characteristics of the rift valley with the
308 proximity to the Afar triangle (Fig. 9). Instead, the rift valley goes through an elevated dome peaking
309 approximately 400 km from the triple junction (Fig. 9a). The along-strike profile (profile B in Fig. 9) shows
310 that the rift valley reaches altitudes of more than 2000 m and is associated with a BGA low.



311 In the Afar triangle, the morphology indicates several axial segments, which are also distinctive in the VGG
312 map (Fig. 10). We recognize axial trends in two distinguished and geographically separated regions: (1)
313 southwest to the Tendaho-Goba'ad Discontinuity, a NE trending valley continues the trend of the Main
314 Ethiopian Rift, characterized by distinct central volcanoes along with an axial depression. (2) Northeast to
315 the Tendaho-Goba'ad Discontinuity, typical rift axial morphologies, composed of NW trending short
316 segments along volcanic ranges, are abundant over a 200 km wide zone. Hence, the Afar depression is
317 divided into two morphological regions, in terms of axial trends, parallel to the Main Ethiopian Rift trending
318 region and parallel to the Red Sea trending region.

319 In summary, with the proximity to the Afar depression the rift axes of the Red Sea and the Gulf Aden are
320 not persistent and drastically change their characteristics ~400 km from the triple junction. In contrast,
321 the axis of the Main Ethiopian Rift is consistent, keeping its trend and characteristics up to the triple
322 junction point.

323 7. Discussion

324 7.1. *The architecture of the intersection region*

325 The Afar triangle is the intersection region of three rift arms, the Gulf of Aden, the Red Sea and the Main
326 Ethiopian Rift. Far from the intersection region, the axes and margins of these rifts follow a general parallel
327 trend suggesting that rigid plate tectonics of the Nubian, Arabian and Somalian plates controlled their
328 structural development (Garfunkel and Beyth, 2006; Reilinger et al., 2006; Reilinger and McClusky, 2011;
329 Schettino et al., 2018). Within the Afar triangle, southwest to the Tendaho-Goba'ad discontinuity, the rift
330 margins are continuous and smooth, and the axial volcanic range generally continues the trend of the axial
331 valley of the Main Ethiopian Rift, reflecting a sub-perpendicular extension in accordance with the Nubia –
332 Somalia kinematics, and thus, could be regarded as a rigid plate boundary. However, the architecture of
333 the intersection region northeast to the Tendaho-Goba'ad discontinuity is more complex and is not simply
334 resolved by rigid plate kinematics (Garfunkel and Beyth, 2006). Fig. 11 summarizes the rift margins and the
335 axial segments mapped in this study. The rift axes of the Gulf of Aden and the Red Sea abruptly change
336 their characteristics, particularly their trends, with the proximity to the Afar region. Around ~400 km from
337 the triple junction, both the Gulf of Aden and the Red Sea axes deviate from their basin parallel trend,
338 bending towards the third and younger arm of the Main Ethiopian Rift. The rift margins within Afar,
339 northeast to the Tendaho-Goba'ad discontinuity, are fragmented, and there are multiple, short, and sub-
340 parallel axial segments. Axial segments are generally sub-parallel to the Red Sea axis and not to the rift
341 margins, which led authors to suggest that this region reflects an evolving discontinuity of the oceanic
342 spreading center in the Red Sea (e.g. Tazieff et al., 1972; Bosworth et al., 2005). However, we don't find
343 any evidence for a transform connection between the ridge in the Red Sea and the continuation of the
344 northern Afar axial segments, offshore Gulf of Zula. Magnetic stripes in the Red Sea are observed at more
345 than 200 km south of the Gulf of Zula region (Fig 12.), and the volcanic ridge in the southern Red Sea is
346 very active (Eyles et al., 2018). Although earthquake clusters at latitude 16.5° indicate strike-slip solutions,
347 supporting a structural connection to the Red Sea axis, these are abundant throughout the study area
348 (Hofstetter and Beyth, 2003). Alternatively, it is possible to regard the jump between the Red Sea ridge to
349 the axial segments in northeastern Afar as a non-transform discontinuity. However, second-order
350 discontinuities are usually characterized by <30 km offsets, and here the jump is of ~200 km (Macdonald
351 et al., 1984; Carbotte et al., 2016). Thus, we find no circumstantial evidence to regard the axial volcanism



352 in the Afar depression as part of the development of the Red Sea spreading center. Our analyses suggest
353 that the area northeast to the Tendaho-Goba'ad discontinuity is characterized by diffuse deformation,
354 reflecting a rugged connection of the Red Sea and the Gulf of Aden arms to the Main Ethiopian Rift.
355 Kinematic studies support this view, indicating that microplate rotations and diffuse boundaries
356 significantly influence the structural development of this region. A recent model based on GPS
357 observations (Viltres et al., 2020) reveals a diffuse character of the Danakil - Nubia boundary with inter-
358 rifting deformation over more than 100 km wide zone. The Danakil microplate extends to Hanish-Zukur
359 Islands at its southern edge (~13.8°N) with no precise/sharp boundary. The Danakil microplate is rotating
360 counterclockwise (Manighetti et al., 2001), while the Ali-Sabieh block, south of the Gulf of Tadjoura, is
361 rotating clockwise (Audin et al., 2004), described as a "saloon-doors" mode of opening (Kidane, 2016).
362 Hence, the architecture of the intersection region of the rift arms discloses a ~150,000 km² complex region,
363 in which the three rift arms are linked by diffuse boundaries and microplate rotations (Fig. 11). Accordingly,
364 a truly single triple junction point, in the sense of a three-rift arms intersection point, cannot be specified
365 for this system, and multiple triple junctions could be considered (e.g., see tectonic models in Viltres et
366 al., 2020). Nevertheless, we agree that the intersection point of the Ethiopian rift valley and the Tendaho-
367 Goba'ad Discontinuity could be regarded as the 'main' junction point of the rift system, as the deformation
368 characteristics are most distinctively changed there (Tsfaye et al., 2003).

369 *7.2. Spatial constraints in the development of the plume-rift system*

370 The architecture of the Afar region allows us to draw two spatial constraints in the development of the
371 plume-rift system:

372 1) The first is the connection of the Main Ethiopian Rift to the Gulf of Aden-Red Sea rifts by a northeastward
373 propagation. The margins of southeast Afar show symmetric, continuous, and smooth curved trends, from
374 the elevated regions of the Main Ethiopian Rift to the Tendaho-Goba'ad Discontinuity (Fig. 6). The
375 Somalian margin is curved clockwise, like the Ali-Sabieh sense of rotation (Kidane, 2016), whereas, the
376 Ethiopian margin is curved counterclockwise, like the Danakil sense of rotation (Schult, 1974). This
377 architecture could be understood in terms of fracture mechanics by reorientation of a propagating fracture
378 in the vicinity of a pre-existing fracture. Strain analysis indicates that a propagating fracture would curve
379 in parallel to the pre-existing fracture under tensional stress field due to free surface boundary conditions
380 induced by the open pre-existing fracture (Dyer, 1988). Thus, this macro scale architecture may express a
381 smooth linkage of the Main Ethiopian Rift to the pre-existing Gulf of Aden-Red Sea rifts by a northeastward
382 propagation. Hence, this implies that a triple junction formed at a late stage, when all the three arms were
383 already significantly developed. This conclusion agrees with structural geochronology within the northern
384 Main Ethiopian Rift showing that extension in the northern Main Ethiopian rift commenced at 11 Ma
385 (Wolfenden et al., 2004).

386 2) The second spatial constraint is an abandonment of an early tectonic connection between the Red Sea
387 and the Gulf of Aden through Bab al-Mandab Strait. As the VGG and neovolcanic activity indicate that the
388 Red Sea axis currently enters Afar at the Bay of Beylul (see section 6.2), we find arguments for an earlier
389 tectonic connection between the Red Sea and the Gulf of Aden through Bab al-Mandab Strait: (i) Below
390 latitude 13.2° and up to the connection to the Gulf of Aden (at latitude 12.3°), the gravity data shows
391 typical rift axis characteristics, with BGA high and VGG picks to its side (Fig. 7 and Fig. 8; see section 6.2).
392 (ii) Submarine channel north to the Hanish Island (latitude 13.4°) has no association with water currents
393 and is best explained by subsurface rift structures (Mitchell and Sofianos, 2018). (iii) This is the straight
394 continuation of the trend of the Red Sea axis, along which the basins are curly connected (Fig. 1). Thus, it



395 is reasonable that it was also the tectonic connection in the early stages of rift development. Likewise,
396 reconstructions suggest that the Danakil microplate started to rotate in Oligocene-Miocene when Arabia
397 was already separated from Africa (Collet et al., 2000). This suggests that the present deviation from the
398 basin parallel trend of the rift axes at the tip of the Gulf of Aden and of the Red Sea marks a tectonic
399 reorganization in this region.

400 These two spatial constraints, the connection of the Main Ethiopian Rift to the Gulf of Aden and to the Red
401 Sea by a northeastward propagation, and, the abandonment of an early tectonic connection between the
402 Red Sea and the Gulf of Aden, indicate that the onset of the triple junction happened at a late stage when
403 the three rift arms were already developed and the Red Sea was tectonically connected to the Gulf of
404 Aden, far (~250 km) from the present-day triple junction (Fig. 13). The onset of the triple junction marks a
405 tectonic reorganization and microplate formation. As a result, the Gulf of Aden and the Red Sea arms are
406 not smoothly connected to the Main Ethiopian Rift, and a vast area of diffuse and complex deformation
407 developed within the intersection region.

408 *7.3. Mechanisms for plume-rift association*

409 The temporal constraints regarding the development of the plume-rift features, summarized in section 4,
410 together with the two spatial constraints inferred in this study, allow us to examine the causal relationship
411 between the activity of the Afar plume and rifting. Our insights suggest that neither ‘active’ nor ‘passive’
412 rifting mechanisms are solely consistent with the observation. Passive rifting models fail to explain the
413 plume-rift association mostly because the flood basalt volcanism cannot be attributed to passively rising
414 asthenospheric mantle beneath a stretched and thinned lithosphere, as dynamic uplift in Ethiopia was
415 shown to be a long-lasting process, prior to flood basalts volcanism (Sembroni et al., 2016). Hence, rifting
416 and associated subsidence is subsequent to flood basalts volcanism (Fig. 4). The estimations of ~1 km
417 elevation prior to flood basalts (Fig. 4) coincide with active plume-head predictions (Campbell and Griffiths,
418 1990). Moreover, the passive model does not provide an explanation why a triple junction is located within
419 the flood basalts area, as rifting in the Red Sea and Gulf of Aden are at an oblique angle to the former
420 sutures (Buitter and Torsvik, 2014).

421 Active models, on the other hand, are not in line with the progressive development of the rifts, mainly
422 because the flood basalts region cannot be considered a center or a nucleus, from which rift arms spread,
423 as expected in an actively generated triple junction. The triple junction was the last feature to develop in
424 the system, by the propagation of the Main Ethiopian Rift towards Afar, followed by a tectonic
425 reorganization including the abandonment of a former tectonic connection between the Red Sea and the
426 Gulf of Aden. By this time, the rift arms were already developed and break-up was already accomplished
427 between Africa and Arabia. This tectonic reorganization cannot be attributed to the development of
428 gravitational potential by the plume head (Hill, 1991), as it occurred millions of years after flood basalts
429 magmatism. That rules out the possibility that the onset of the triple junction was generated by the arrival
430 of the Afar plume, as more than 20 Ma separate these events, and as the rift arms did not spread from the
431 plume region.

432 We propose a scenario in which rifting was triggered by a plume-induced plate rotation (Fig. 2c). Numerical
433 simulations suggest that horizontal asthenospheric flows due to the arrival of a plume-head at the base of
434 the lithosphere induce a plume-push force that can accelerate plates by several cm yr^{-1} (van Hinsbergen
435 et al., 2011, 2021; Pusok and Stegman, 2020). In this scenario, flood basalt volcanism would be
436 synchronous to an abrupt plate speed-up and thus to new remote stress conditions. In the case of the



437 Indian plate, at least two episodes of massive flood basalt volcanism, Morondava LIP (~94 Ma) and Deccan
438 traps (67 Ma), are associated with plume derived plate acceleration, and a drastic change in the tectonic
439 framework (van Hinsbergen et al., 2011, 2021; Cande and Stegman, 2011; Pusok and Stegman, 2020).
440 Further, torque balance modeling suggests that horizontal plume-push can force a significant plate
441 rotation and, consequently the initiation of new plate boundaries (van Hinsbergen et al., 2021).

442 In the Afro-Arabian rift, indeed new plate boundaries formed after the arrival of the large Afar plume and
443 a significant plate rotation of Arabia around a nearby pole characterizes the Arabian continent (Joffe and
444 Garfunkel, 1987; Viltres et al., 2022). Magnetic stripes and structural reconstructions suggest that the
445 rotation around a nearby pole already characterizes Arabia since the Oligocene (Fournier et al., 2010;
446 Schettino et al., 2018). Additionally, the beginning of intensive volcanism in the north-western Arabian
447 plate (Harrat Ash Shaam) at Late Oligocene (Ilani et al., 2001), reflecting a change in mantle-crust
448 interaction and in intracontinental extension within the Arabian plate, adjacent to the arrival of Afar plume
449 (Garfunkel, 1989). In this large volcanic field, diking directions from Miocene to recent ages record the
450 rotation of Arabia (Giannerini et al., 1988), suggesting that already during the first stages of volcanism the
451 Arabian plate was rotating around a nearby pole. The arrival of the Afar plume was also accompanied by
452 a slowdown of Africa (Le Pichon and Gaulier, 1988). By this time, Africa collided with Eurasia in the west,
453 explaining its slowdown (Jolivet and Faccenna, 2000) and its increased intraplate volcanism (Burke, 1996).
454 However, this collision of Africa and Eurasia cannot simply resolve the change in the rotation of Arabia as
455 the Arabian continent collided with Eurasia no earlier than ~18 Ma (Su and Zhou, 2020), although some
456 authors suggested that asymmetrical along-trench entrance of continental material could lead to an
457 intraplate extension similar to those that generated the Africa-Arabia break-up (Bellahsen et al., 2003).
458 Faccenna et al., (2013) already showed that plume-push from the Afar area resolves the present-day plate
459 kinematics in the middle-east, particularly the anti-clockwise toroidal pattern of the Arabia–Anatolia–
460 Aegean system. The importance of active upwelling in Afar to lateral mantle flow below Arabia is also
461 illustrated by shear-wave splitting indicating a general N-S anisotropy in the mantle (Qaysi et al., 2018).

462 If the rotation of Arabia around a nearby pole was induced by the Afar plume, then it is understood how
463 the Gulf of Aden and the Red Sea rifts developed after a regional uplift and flood basalt volcanism but still
464 geometrically developed by the new regional stress field and structural inheritance (Autin et al., 2013;
465 Bosworth and Stockli, 2016). It also provides an explanation of why the trace of the rifts intersect within
466 the plume region as the lithosphere in this region was weakened by the hot plume material (François et
467 al., 2018). Finally, it explains the delayed development of the Main Ethiopian Rift and the late onset of the
468 Afar triple junction by its northwestward propagation, as these were controlled by the slower kinematics
469 of the Somalian plate rather than dynamic forces. In this manner, ‘active’ and ‘passive’ mechanisms are
470 coupled and have a positive feedback, allowing a close occurrence of flood basalts volcanism and
471 continental break-up, alongside a passive style of rifting.

472 8. Summary and Conclusions

473 We reviewed the geologic setting of the Afro-Arabian rift, in which vast regions of flood basalts and an
474 ongoing continental break-up are superimposed, aiming to infer causal relationship between the activity
475 of the deep seated Afar plume and crustal break-up. We explored the intersection region in which the Gulf
476 of Aden, the Red Sea and the Main Ethiopian Rift form an R-R-R triple junction, separating the large
477 Cenozoic plume related flood basalt series in Ethiopia and Yemen. We provide a new synthesis and



478 interpretation to modern geophysical datasets including topography, bathymetry, gravity, magnetic
479 anomalies, earthquakes and volcano distribution to map the margins and axes of the rift arms.

480 We highlight key differences in the terminations of the Gulf of Aden and the Red Sea arms, which are rough
481 and irregular, versus the symmetric, continuous, and smooth architecture of the Main Ethiopian Rift. The
482 architecture of the intersection regions allows us to infer two tempo-spatial constraints in the
483 development of the rifts: (1) the connection of the Main Ethiopian Rift to the Gulf of Aden and to the Red
484 Sea by its northeastward propagation, and, (2) the abandonment of an early tectonic connection between
485 the Red Sea and the Gulf of Aden. These suggest a progressive development of the intersection area
486 including a broad region of diffuse deformation and recent tectonic reorganization. The onset of the triple
487 junction was the last feature to develop in the plume-rift system, after all rift arms were sufficiently
488 developed and break-up was accomplished.

489 This progressive development is not in line with the classic active rifting model, which predicts a plume-
490 generated triple junction at the locus of the rift, from which the rifts develop. Nevertheless, the classic
491 passive rifting model fails to explain the chronological evidence as flood basalts probably erupted on
492 elevated topography before rifting started. We discuss a scenario of plume-induced plate rotation in which
493 the rotation of Arabia around a nearby pole was triggered by the arrival of the Afar plume. We
494 demonstrate that the rotation of Arabia around a nearby pole characterizes the system since the Oligocene
495 and reflects observed mantle flows below Arabia. We suggest that this scenario better explains the
496 progressive development of the plume-rift system in the Afro-Arabian rift.

497 9. Data availability

498 The bathymetry and topography data used in this study was retrieved from GEBCO Compilation Group
499 (2021), available at https://www.gebco.net/data_and_products/gridded_bathymetry_data/#area.

500 The VGG data used in this study is available at https://topex.ucsd.edu/grav_outreach/.

501 The BGA data used in this study is available at <http://icgem.gfz-potsdam.de/calcrgrid>; model XGM2019e-
502 2159, 'gravity_anomaly_bg'.

503 Earthquake data was retrieved from the International Seismological Centre (2020), On-line Bulletin,
504 <https://doi.org/10.31905/D808B830>.

505 Quaternary onshore volcano locations were retrieved from the Global Volcanism Program, Smithsonian
506 Institution, available at https://volcano.si.edu/volcanolist_holocene.cfm.

507 10. Author contribution

508 RI carried out the study and wrote and revised the original draft of this paper. PH and NA provided a
509 conceptual assistance, helped in writing and reviewed the manuscript. JE mentored the study, took care
510 of administration and reviewed the manuscript.



511 11. Competing interests

512 The contact author has declared that neither of the authors has any competing interests.

513 12. Acknowledgments

514 This work was supported by the grants from Minerva Fellowship to R. I.

515 13. Figure captions

516 **Fig. 1.** Elevation map of the study area, showing the general plate tectonic configuration (from USGS and
517 from Viltres et al. (2020) in the Afar region) and Cenozoic volcanics (modified from Varet, 1978; Davison
518 et al., 1994; Beyene and Abdelsalam, 2005; Bosworth and Stockli, 2016) Black arrows indicate GPS
519 velocities in respect to Nubia (modified from Reilinger et al., 2006).

520 **Fig. 2.** Schematic mechanisms for plume-rift association in the Afro-Arabian rift. (a) Active mechanism, in
521 which rifting results from the actively rising head of the Afar plume. In this mechanism impinging and
522 eroding the base of the lithosphere prompt uplift and decompression melting and flood basalts volcanism.
523 These introduce internal extensional forces and ultimately lead to break-up. (b) Passive mechanism, in
524 which rifting is initiated solely by the remote stresses, regardless of underlying Afar plume. In this
525 mechanism the production of massive volcanism is allowed when the thinned and stretched lithosphere
526 is underlaid by the thermal anomaly in the mantle. Flood basalts volcanism is generated by passively rising
527 decompression melting of hot asthenospheric mantle. (c) Plume-induced plate rotation, in which lateral
528 forces, induced by the arrival of the Afar plume head, add up to the remote stresses to change the plate
529 kinematics. In this mechanism flood basalts volcanism is actively controlled, however, rifting is triggered
530 by the new plate kinematics.

531 **Fig. 3.** Map of the Afar region showing magnetic isochrons (modified from Fournier et al., 2010; Bridges et
532 al., 2012; Schettino et al., 2016), earthquake locations (from ISC catalog), Holocene onshore volcano
533 locations (from GVP catalog and Viltres et al., (2020)) and recent volcanism (modified from Keir et al.,
534 2013).

535 **Fig. 4.** Elevation of the Ethiopian–Yemen plateau (after Sembroni et al., 2016; Faccenna et al., 2019),
536 volcanic episodes and opening rates of the rift arms (modified from Fournier et al., 2010; DeMets and
537 Merkouriev, 2016; Schettino et al., 2018). Dashed lines indicate estimations from geological observations
538 and solid lines from magnetic isochrons.

539 **Fig. 5.** Gravity data of the Afar region. (a) Vertical gravity gradient from Sandwell et al. (2014). Bouguer
540 anomaly model from ICGEM, XGM2019e (Zingerle et al., 2020).

541 **Fig. 6.** (a) Difference of Gaussians applied to topography and bathymetry showing rift margins (black lines).
542 White dashed lines indicate peaks in rift width. TGD is the Tendaho-Goba’ad Discontinuity. SSD is the
543 Shukra al Sheik discontinuity. Black dots indicate earthquake locations (ISC catalog). (b) Rift widths,
544 calculated in rift-perpendicular directions.



- 545 **Fig. 7.** Bathymetry (a), vertical gravity gradient (b) and Bouguer anomaly (c) in the southern Red Sea. Black
546 dots indicate earthquake locations (ISC catalog). (d) Profiles across rift axis.
- 547 **Fig. 8.** Bathymetry (a), vertical gravity gradient (b) and Bouguer anomaly (c) in the Western Gulf of Aden.
548 Black dots indicate earthquake locations (ISC catalog). (d) Profiles across rift axis.
- 549 **Fig. 9.** Topography (a), vertical gravity gradient (b) and Bouguer anomaly (c) in the northern Main Ethiopian
550 Rift. Black dots indicate earthquake locations (ISC catalog). (d) Profiles across (AA') and along (BB') the rift
551 valley.
- 552 **Fig. 10.** Topography (a), vertical gravity gradient (b) and Bouguer anomaly (c) in the Afar triangle. Black
553 dots indicate earthquake locations (ISC catalog). TGD is the Tendaho-Goba'ad Discontinuity. (d) Profiles
554 SW (AA') and NE (BB') to the TGD.
- 555 **Fig. 11.** Rift margins (solid white lines) and axial segments (long dashed black lines) in the Afar region. Black
556 dots indicate earthquake locations (ISC catalog). TGD is the Tendaho-Goba'ad Discontinuity.
- 557 **Fig. 12.** Tilt-angle derivative map of magnetic anomalies, projected on a shaded relief after Issachar et al.
558 (2022). Purple colures represent positive angles and green colors represent negative angles. White dashed
559 lines indicate magnetic stripes (Schettino et al., 2016).
- 560 **Fig. 13.** Synthesis of the progressive development of the rift intersections.

561 14. References

- 562 Akram, F., Garcia, M.A., and Puig, D., 2017, Active contours driven by difference of Gaussians: Scientific
563 Reports, v. 7, p. 1–15, doi:10.1038/s41598-017-14502-w.
- 564 Audin, L., Quidelleur, X., Coulié, E., Courtillot, V., Gilder, S., Manighetti, I., Gillot, P.Y., Tapponnier, P., and
565 Kidane, T., 2004, Palaeomagnetism and K-Ar and 40 Ar/39 Ar ages in the Ali Sabieh area (Republic of
566 Djibouti and Ethiopia): Constraints on the mechanism of Aden ridge propagation into southeastern
567 Afar during the last 10 Myr: Geophysical Journal International, v. 158, p. 327–345,
568 doi:10.1111/j.1365-246X.2004.02286.x.
- 569 Augustin, N., van der Zwan, F.M., Devey, C.W., and Brandsdóttir, B., 2021, 13 million years of seafloor
570 spreading throughout the Red Sea Basin: Nature Communications, v. 12, p. 1–10,
571 doi:10.1038/s41467-021-22586-2.
- 572 Autin, J., Bellahsen, N., Leroy, S., Husson, L., Beslier, M.O., and d'Acremont, E., 2013, The role of structural
573 inheritance in oblique rifting: Insights from analogue models and application to the Gulf of Aden:
574 Tectonophysics, v. 607, p. 51–64, doi:10.1016/J.TECTO.2013.05.041.
- 575 Bellahsen, N., Faccenna, C., Funiciello, F., Daniel, J.M., and Jolivet, L., 2003, Why did Arabia separate from
576 Africa? Insights from 3-D laboratory experiments: Earth and Planetary Science Letters, v. 216, p. 365–
577 381, doi:10.1016/S0012-821X(03)00516-8.
- 578 Bellahsen, N., Husson, L., Autin, J., Leroy, S., and D'Acremont, E., 2013, The effect of thermal weakening
579 and buoyancy forces on rift localization: Field evidences from the Gulf of Aden oblique rifting:
580 Tectonophysics, v. 607, p. 80–97, doi:10.1016/j.tecto.2013.05.042.
- 581 Bellieni, G., Visentin, E.J., Zanettin, B., Piccirillo, E.M., Radicati di Brozolo, F., and Rita, F., 1981, Oligocene



- 582 transitional tholeiitic magmatism in Northern turkana (Kenya): Comparison with the Coeval Ethiopian
583 volcanism: *Bulletin Volcanologique*, v. 44, p. 411–427, doi:10.1007/BF02600573.
- 584 Beyene, A., and Abdelsalam, M.G., 2005, Tectonics of the Afar Depression: A review and synthesis: *Journal*
585 *of African Earth Sciences*, v. 41, p. 41–59, doi:10.1016/j.jafrearsci.2005.03.003.
- 586 Bosworth, W., 2015, Geological evolution of the Red Sea: historical background, review, and synthesis, *in*
587 *In The Red Sea*, Springer, Berlin, Heidelberg, p. 45–78, doi:10.1007/978-3-662-45201-1.
- 588 Bosworth, W., Huchon, P., and McClay, K., 2005, The Red Sea and Gulf of Aden Basins: *Journal of African*
589 *Earth Sciences*, v. 43, p. 334–378, doi:10.1016/j.jafrearsci.2005.07.020.
- 590 Bosworth, W., and Stockli, D.F., 2016, Early magmatism in the greater Red Sea rift: Timing and significance:
591 *Canadian Journal of Earth Sciences*, v. 53, p. 1158–1176, doi:10.1139/cjes-2016-0019.
- 592 Bridges, D.L., Mickus, K., Gao, S.S., Abdelsalam, M.G., and Alemu, A., 2012, Magnetic stripes of a
593 transitional continental rift in Afar: *Geology*, v. 40, p. 203–206, doi:10.1130/G32697.1.
- 594 Bryan, S.E., and Ferrari, L., 2013, Large igneous provinces and silicic large igneous provinces: Progress in
595 our understanding over the last 25 years: *GSA Bulletin*, v. 125, p. 1053–1078, doi:10.1130/B30820.1.
- 596 Buiter, S.J.H., and Torsvik, T.H., 2014, A review of Wilson Cycle plate margins: A role for mantle plumes in
597 continental break-up along sutures? *Gondwana Research*, v. 26, p. 627–653,
598 doi:10.1016/J.GR.2014.02.007.
- 599 Burke, K., 1996, The African Plate: *South African Journal of Geology*, v. 99, p. 341–409, doi:10.10520/EJC-
600 942801F20.
- 601 Burke, K., and Dewey, J.F., 1973, Plume-generated triple junctions: key indicators in applying plate
602 tectonics to old rocks: *The Journal of Geology*, v. 81, p. 406–433,
603 doi:https://doi.org/10.1086/627882.
- 604 Campbell, I.H., and Griffiths, R.W., 1990, Implications of mantle plume structure for the evolution of flood
605 basalts: *Earth and Planetary Science Letters*, v. 99, p. 79–93, doi:10.1016/0012-821X(90)90072-6.
- 606 Cande, S.C., and Stegman, D.R., 2011, Indian and African plate motions driven by the push force of the
607 Réunion plume head: *Nature*, v. 475, p. 47–52, doi:10.1038/nature10174.
- 608 Carbotte, S.M., Smith, D.K., Cannat, M., and Klein, E.M., 2016, Tectonic and magmatic segmentation of the
609 Global Ocean Ridge System: A synthesis of observations, *in Geological Society Special Publication*,
610 *Geological Society of London*, v. 420, p. 249–295, doi:10.1144/SP420.5.
- 611 Chatterjee, S., Goswami, A., and Scotese, C.R., 2013, The longest voyage: Tectonic, magmatic, and
612 paleoclimatic evolution of the Indian plate during its northward flight from Gondwana to Asia:
613 *Gondwana Research*, v. 23, p. 238–267, doi:10.1016/j.gr.2012.07.001.
- 614 Chorowicz, J., 2005, The East African rift system: *Journal of African Earth Sciences*, v. 43, p. 379–410,
615 doi:10.1016/j.jafrearsci.2005.07.019.
- 616 Collet, B., Taud, H., Parrot, J.F., Bonavia, F., and Chorowicz, J., 2000, A new kinematic approach for the
617 Danakil block using a Digital Elevation Model representation: *Tectonophysics*, v. 316, p. 343–357,
618 doi:10.1016/S0040-1951(99)00263-2.
- 619 Corti, G., 2009, Continental rift evolution: From rift initiation to incipient break-up in the Main Ethiopian
620 Rift, East Africa: *Earth-Science Reviews*, v. 96, p. 1–53, doi:10.1016/j.earscirev.2009.06.005.
- 621 Coulié, E., Quidelleur, X., Courtillot, V., Lefèvre, J.C., and Chiesa, S., 2003, Comparative K-Ar and Ar/Ar
622 dating of Ethiopian and Yemenite Oligocene volcanism: Implications for timing and duration of the



- 623 Ethiopian traps: *Earth and Planetary Science Letters*, v. 206, p. 477–492, doi:10.1016/S0012-
624 821X(02)01089-0.
- 625 Courtillot, V., Jaupart, C., Manighetti, I., Tapponnier, P., and Besse, J., 1999, On causal links between flood
626 basalts and continental breakup: *Earth and Planetary Science Letters*, v. 166, p. 177–195,
627 doi:10.1016/S0012-821X(98)00282-9.
- 628 Davison, I. et al., 1994, Geological evolution of the southeastern Red Sea Rift margin, Republic of Yemen:
629 *Geological Society of America Bulletin*, v. 106, p. 1474–1493, doi:10.1130/0016-
630 7606(1994)106<1474:GEOTSR>2.3.CO;2.
- 631 DeMets, C., and Merkouriev, S., 2016, High-resolution estimates of Nubia-Somalia plate motion since 20
632 Ma from reconstructions of the Southwest Indian Ridge, Red Sea and Gulf of Aden: *Geophysical*
633 *Journal International*, v. 207, p. 317–332, doi:10.1093/gji/ggw276.
- 634 Duclaux, G., Huismans, R.S., and May, D.A., 2020, Rotation, narrowing, and preferential reactivation of
635 brittle structures during oblique rifting: *Earth and Planetary Science Letters*, v. 531, p. 115952,
636 doi:10.1016/j.epsl.2019.115952.
- 637 Dyer, R., 1988, Using joint interactions to estimate paleostress ratios: *Journal of Structural Geology*, v. 10,
638 p. 685–699, doi:10.1016/0191-8141(88)90076-4.
- 639 Ernst, R.E., 2014, *Large igneous provinces*: Cambridge University Press.
- 640 Eyles, J.H.W., Illsley-Kemp, F., Keir, D., Ruch, J., and Jónsson, S., 2018, Seismicity Associated With the
641 Formation of a New Island in the Southern Red Sea: *Frontiers in Earth Science*, v. 6, p. 1–10,
642 doi:10.3389/feart.2018.00141.
- 643 Faccenna, C., Becker, T.W., Jolivet, L., and Keskin, M., 2013, Mantle convection in the Middle East:
644 Reconciling Afar upwelling, Arabia indentation and Aegean trench rollback: *Earth and Planetary*
645 *Science Letters*, v. 375, p. 254–269, doi:10.1016/J.EPSL.2013.05.043.
- 646 Faccenna, C., Glišović, P., Forte, A., Becker, T.W., Garzanti, E., Sembroni, A., and Gvirtzman, Z., 2019, Role
647 of dynamic topography in sustaining the Nile River over 30 million years: *Nature Geoscience*, v. 12,
648 p. 1012–1017, doi:10.1038/s41561-019-0472-x.
- 649 Fournier, M. et al., 2010, Arabia-Somalia plate kinematics, evolution of the Aden-OwenCarlsberg triple
650 junction, and opening of the Gulf of Aden: *Journal of Geophysical Research: Solid Earth*, v. 115, p. 1–
651 24, doi:10.1029/2008JB006257.
- 652 François, T., Koptev, A., Cloetingh, S., Burov, E., and Gerya, T., 2018, Plume-lithosphere interactions in
653 rifted margin tectonic settings: Inferences from thermo-mechanical modelling: *Tectonophysics*, v.
654 746, p. 138–154, doi:10.1016/j.tecto.2017.11.027.
- 655 Frizon De Lamotte, D., Fourdan, B., Leleu, S., Leparmentier, F., and De Clarens, P., 2015, Style of rifting and
656 the stages of Pangea breakup: *Tectonics*, v. 34, p. 1009–1029, doi:10.1002/2014TC003760.
- 657 Fromm, T., Planert, L., Jokat, W., Ryberg, T., Behrmann, J.H., Weber, M.H., and Haberland, C., 2015, South
658 Atlantic opening: A plume-induced breakup? *Geology*, v. 43, p. 931–934, doi:10.1130/G36936.1.
- 659 Garfunkel, Z., 1989, Tectonic setting of phanerozoic magmatism in Israel: *Israel journal of earth-sciences*,
660 v. 38, p. 51–74.
- 661 Garfunkel, Z., and Beyth, M., 2006, Constraints on the structural development of Afar imposed by the
662 kinematics of the major surrounding plates: *Geological Society Special Publication*, v. 259, p. 23–42,
663 doi:10.1144/GSL.SP.2006.259.01.04.



- 664 GEBCO Compilation Group, 2021, The GEBCO_2019 Grid: a continuous terrain model of the global oceans
665 and land:, doi:10.5285/c6612cbe-50b3-0cff-e053-6c86abc09f8f.
- 666 Geoffroy, L., 2005, Volcanic passive margins: *Comptes Rendus Geoscience*, v. 337, p. 1395–1408,
667 doi:10.1016/J.CRTE.2005.10.006.
- 668 George, R., Rogers, N., and Kelley, S., 1998, Earliest magmatism in Ethiopia: Evidence for two mantle
669 plumes in one flood basalt province: *Geology*, v. 26, p. 923–926, doi:10.1130/0091-
670 7613(1998)026<0923:EMIEEF>2.3.CO;2.
- 671 Giannerini, G., Campredon, R., Feraud, G., and Abou Zakhem, B., 1988, Deformations intraplaques et
672 volcanisme associe; exemple de la bordure NW de la plaque Arabique au Cenozoique: *Bulletin de la*
673 *Société Géologique de France*, v. IV, p. 937–947, doi:10.2113/gssgfbull.IV.6.937.
- 674 Gillard, M., Leroy, S., Cannat, M., and Sloan, H., 2021, Margin-to-Margin Seafloor Spreading in the Eastern
675 Gulf of Aden: A 16 Ma-Long History of Deformation and Magmatism from Seismic Reflection, Gravity
676 and Magnetic Data: *Frontiers in Earth Science*, v. 9, p. 628, doi:10.3389/feart.2021.707721.
- 677 Gvirtzman, Z., Faccenna, C., and Becker, T.W., 2016, Isostasy, flexure, and dynamic topography:
678 *Tectonophysics*, v. 683, p. 255–271, doi:10.1016/j.tecto.2016.05.041.
- 679 Hill, R.I., 1991, Starting plumes and continental break-up: *Earth and Planetary Science Letters*, v. 104, p.
680 398–416, doi:10.1016/0012-821X(91)90218-7.
- 681 van Hinsbergen, D.J.J. et al., 2021, A record of plume-induced plate rotation triggering subduction
682 initiation: *Nature Geoscience*, v. 14, p. 626–630, doi:10.1038/s41561-021-00780-7.
- 683 van Hinsbergen, D.J.J., Steinberger, B., Doubrovine, P. V., and Gassmöller, R., 2011, Acceleration and
684 deceleration of India-Asia convergence since the Cretaceous: Roles of mantle plumes and continental
685 collision: *Journal of Geophysical Research: Solid Earth*, v. 116, p. 6101, doi:10.1029/2010JB008051.
- 686 Hofstetter, R., and Beyth, M., 2003, The afar depression: Interpretation of the 1960-2000 earthquakes:
687 *Geophysical Journal International*, v. 155, p. 715–732, doi:10.1046/j.1365-246X.2003.02080.x.
- 688 Hughes, G.W., Varol, O., and Beydoun, Z.R., 1991, Evidence for Middle Oligocene rifting of the Gulf of Aden
689 and for Late Oligocene rifting of the southern Red Sea: *Marine and Petroleum Geology*, v. 8, p. 354–
690 358, doi:10.1016/0264-8172(91)90088-I.
- 691 Huisman, R.S., Podladchikov, Y.Y., and Cloetingh, S., 2001, Transition from passive to active rifting:
692 Relative importance of asthenospheric doming and passive extension of the lithosphere: *Journal of*
693 *Geophysical Research: Solid Earth*, v. 106, p. 11271–11291, doi:10.1029/2000JB900424.
- 694 Ilani, S., Harlavan, Y., Tarawneh, K., Rabba, I., Weinberger, R., Ibrahim, K., Peltz, S., and Steinitz, G., 2001,
695 New K-Ar ages of basalts from the Harrat Ash Shaam volcanic field in Jordan: Implications for the
696 span and duration of the upper-mantle upwelling beneath the western Arabian plate: *Geology*, v. 29,
697 p. 171–174, doi:10.1130/0091-7613(2001)029<0171:NKAAOB>2.0.CO;2.
- 698 Ince, E.S., Barthelmes, F., Reißland, S., Elger, K., Förste, C., Flechtner, F., and Schuh, H., 2019, ICGEM – 15
699 years of successful collection and distribution of global gravitational models, associated services, and
700 future plans: *Earth System Science Data*, v. 11, p. 647–674, doi:10.5194/essd-11-647-2019.
- 701 Issachar, R., Ebbing, J., and Dilixiati, Y., 2022, New magnetic anomaly map for the Red Sea reveals
702 transtensional structures associated with rotational rifting: *Scientific Reports*, v. 12, p. 1–13,
703 doi:10.1038/s41598-022-09770-0.
- 704 Ivanov, A. V., Demonterova, E.I., He, H., Perepelov, A.B., Travin, A. V., and Lebedev, V.A., 2015, Volcanism
705 in the Baikal rift: 40years of active-versus-passive model discussion: *Earth-Science Reviews*, v. 148,



- 706 p. 18–43, doi:10.1016/j.earscirev.2015.05.011.
- 707 Joffe, S., and Garfunkel, Z., 1987, Plate kinematics of the Red Sea – a re-evaluation: *Tectonophysics*, v. 141,
708 p. 5–22.
- 709 Jolivet, L., and Faccenna, C., 2000, Mediterranean extension and the Africa-Eurasia collision: *Tectonics*, v.
710 19, p. 1095–1106, doi:10.1029/2000TC900018.
- 711 Keen, C.E., 1985, The dynamics of rifting: deformation of the lithosphere by active and passive driving
712 forces: *Geophys. J. R. astr. Soc.*, v. 80, p. 95–120,
713 <https://academic.oup.com/gji/article/80/1/95/610547> (accessed August 2021).
- 714 Keir, D., Bastow, I.D., Pagli, C., and Chambers, E.L., 2013, The development of extension and magmatism
715 in the Red Sea rift of Afar: *Tectonophysics*, v. 607, p. 98–114, doi:10.1016/j.tecto.2012.10.015.
- 716 Kidane, T., 2016, Strong clockwise block rotation of the Ali-Sabieh/Aïsha Block: Evidence for opening of the
717 Afar Depression by a “saloon-door” mechanism, *in Geological Society Special Publication, Geological*
718 *Society of London*, v. 420, p. 209–219, doi:10.1144/SP420.10.
- 719 Koppers, A.A.P., Becker, T.W., Jackson, M.G., Konrad, K., Müller, R.D., Romanowicz, B., Steinberger, B., and
720 Whittaker, J.M., 2021, Mantle plumes and their role in Earth processes: *Nature Reviews Earth &*
721 *Environment*, v. 2, p. 382–401, doi:10.1038/s43017-021-00168-6.
- 722 Koptev, A., Gerya, T., Calais, E., Leroy, S., and Burov, E., 2018, Afar triple junction triggered by plume-
723 assisted bi-directional continental break-up: *Scientific Reports*, v. 8, p. 1–7, doi:10.1038/s41598-018-
724 33117-3.
- 725 Leroy, S. et al., 2013, From rifting to oceanic spreading in the Gulf of Aden: A synthesis: *Frontiers in Earth*
726 *Sciences*, v. 5, p. 385–427, doi:10.1007/978-3-642-30609-9_20.
- 727 Lithgow-Bertelloni, C., and Silver, P.G., 1998, Dynamic topography, plate driving forces and the African
728 superswell: *Nature*, v. 395, p. 269–272, doi:10.1038/26212.
- 729 Macdonald, K., Sempere, J.C., and Fox, P.J., 1984, East Pacific Rise from Siqueiros to Orozco fracture zones:
730 along-strike continuity of axial neovolcanic zone and structure and evolution of overlapping
731 spreading centers.: *Journal of Geophysical Research*, v. 89, p. 6049–6069,
732 doi:10.1029/JB089iB07p06049.
- 733 Manighetti, I., Tapponnier, P., Courtillot, V., Gallet, Y., Jacques, E., and Gillot, P.Y., 2001, Strain transfer
734 between disconnected, propagating rifts in Afar: *Journal of Geophysical Research: Solid Earth*, v. 106,
735 p. 13613–13665, doi:10.1029/2000jb900454.
- 736 Mattash, M.A., Pinarelli, L., Vaselli, O., Minissale, A., Al-Kadasi, M., Shawki, M.N., and Tassi, F., 2013,
737 Continental Flood Basalts and Rifting: Geochemistry of Cenozoic Yemen Volcanic Province:
738 *International Journal of Geosciences*, v. 04, p. 1459–1466, doi:10.4236/ijg.2013.410143.
- 739 McConnell, R., and Baker, B., 1970, The Structural Pattern of the Afro-Arabian Rift System in Relation to
740 Plate Tectonics: Discussion: *Philosophical Transactions of the Royal Society of London Series A*, v.
741 267, p. 390–391, https://www.jstor.org/stable/73628?seq=3#metadata_info_tab_contents
742 (accessed August 2021).
- 743 McDougall, I. an, and Brown, F.H., 2009, Timing of volcanism and evolution of the northern Kenya Rift:
744 *Geological Magazine*, v. 146, p. 34–47, doi:DOI: 10.1017/S0016756808005347.
- 745 Meshesha, D., and Shinjo, R., 2008, Rethinking geochemical feature of the Afar and Kenya mantle plumes
746 and geodynamics implications: *Journal of Geophysical Research: Solid Earth*, v. 113, p. 9209,
747 doi:10.1029/2007JB005549.



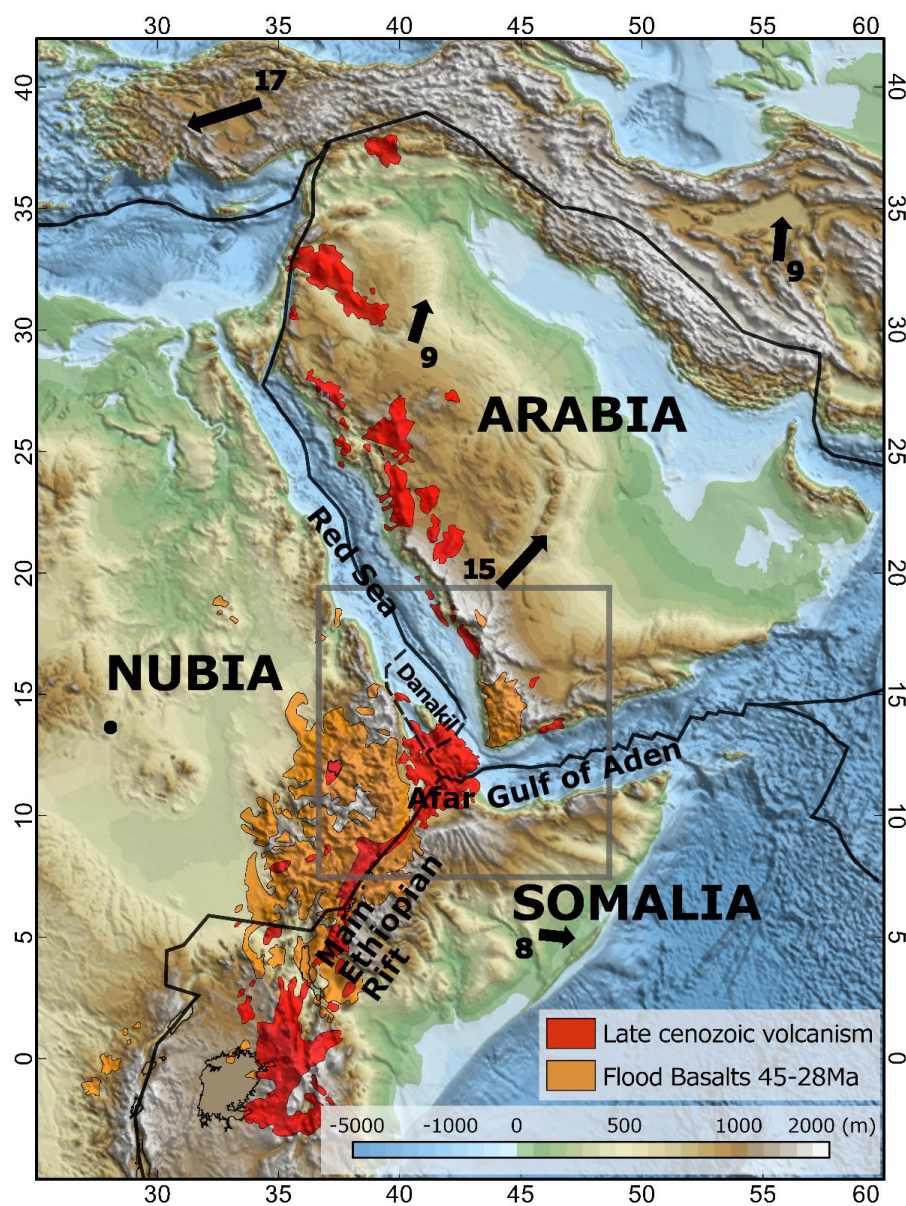
- 748 Mitchell, N.C., and Sofianos, S.S., 2018, Origin of submarine channel north of hanish sill, red sea, *in*
749 Geological Setting, Palaeoenvironment and Archaeology of the Red Sea, Springer International
750 Publishing, p. 259–273, doi:10.1007/978-3-319-99408-6_12.
- 751 Mitra, S., Mitra, K., Gupta, S., Bhattacharya, S., Chauhan, P., and Jain, N., 2017, Alteration and submergence
752 of basalts in Kachchh, Gujarat, India: implications for the role of the Deccan Traps in the India–
753 Seychelles break-up: Geological Society, London, Special Publications, v. 445, p. 47–67,
754 doi:10.1144/SP445.9.
- 755 Morag, N., Haviv, I., Eyal, M., Kohn, B.P., and Feinstein, S., 2019, Early flank uplift along the Suez Rift:
756 Implications for the role of mantle plumes and the onset of the Dead Sea Transform: Earth and
757 Planetary Science Letters, v. 516, p. 56–65, doi:10.1016/j.epsl.2019.03.002.
- 758 Moretti, I., and Froidevaux, C., 1986, Thermomechanical models of active rifting: Tectonics, v. 5, p. 501–
759 511, doi:10.1029/TC005I004P00501.
- 760 Morgan, W.J., 1971, Convection plumes in the lower mantle: Nature, v. 230, p. 42–43,
761 doi:10.1038/230042a0.
- 762 Peate, I.U., Baker, J.A., Al-Kadasi, M., Al-Subbary, A., Knight, K.B., Riisager, P., Thirlwall, M.F., Peate, D.W.,
763 Renne, P.R., and Menzies, M.A., 2005, Volcanic stratigraphy of large-volume silicic pyroclastic
764 eruptions during Oligocene Afro-Arabian flood volcanism in Yemen: Bulletin of Volcanology, v. 68, p.
765 135–156, doi:10.1007/s00445-005-0428-4.
- 766 Le Pichon, X., and Gaulier, J.-M., 1988, The rotation of Arabia and the Levant fault system: Tectonophysics,
767 v. 153, p. 271–294, doi:10.1016/0040-1951(88)90020-0.
- 768 Plaziat, J.-C., Baltzer, F., Choukri, A., Conchon, O., Freytet, P., Orszag-Sperber, F., Raguideau, A., and Reys,
769 J.-L., 1998, Quaternary marine and continental sedimentation in the northern Red Sea and Gulf of
770 Suez (Egyptian coast): influences of rift tectonics, climatic changes and sea-level fluctuations, *in*
771 Sedimentation and Tectonics in Rift Basins Red Sea:- Gulf of Aden, Springer Netherlands, p. 537–573,
772 doi:10.1007/978-94-011-4930-3_29.
- 773 Prave, A.R., Bates, C.R., Donaldson, C.H., Toland, H., Condon, D.J., Mark, D., and Raub, T.D., 2016, Geology
774 and geochronology of the Tana Basin, Ethiopia: LIP volcanism, Super eruptions and Eocene-Oligocene
775 environmental change: Earth and Planetary Science Letters, v. 443, p. 1–8,
776 doi:10.1016/j.epsl.2016.03.009.
- 777 Pusok, A.E., and Stegman, D.R., 2020, The convergence history of India-Eurasia records multiple
778 subduction dynamics processes: Science Advances, v. 6,
779 doi:10.1126/SCIADV.AAZ8681/SUPPL_FILE/AAZ8681_SM.PDF.
- 780 Qaysi, S., Liu, K.H., and Gao, S.S., 2018, A Database of Shear-Wave Splitting Measurements for the Arabian
781 Plate: Seismological Research Letters, v. 89, p. 2294–2298, doi:10.1785/0220180144.
- 782 Reilinger, R. et al., 2006, GPS constraints on continental deformation in the Africa-Arabia-Eurasia
783 continental collision zone and implications for the dynamics of plate interactions: Journal of
784 Geophysical Research-Solid Earth, v. 111.
- 785 Reilinger, R., and McClusky, S., 2011, Nubia-Arabia-Eurasia plate motions and the dynamics of
786 Mediterranean and Middle East tectonics: Geophysical Journal International, v. 186, p. 971–979,
787 doi:10.1111/j.1365-246X.2011.05133.x.
- 788 Richards, M.A., Duncan, R.A., and Courtillot, V.E., 1989, Flood basalts and hot-spot tracks: Plume heads
789 and tails: Science, v. 246, p. 103–107, doi:10.1126/science.246.4926.103.



- 790 Roger, J., Platel, J.P., Cavelier, C., and Bourdillon-de-Grissac, C., 1989, Données nouvelles sur la
791 stratigraphie et l'histoire géologique du Dhofar (Sultanat d'Oman): Bulletin de la Société géologique
792 de France, v. 2, p. 256–277, In France, abstract in English.
- 793 Rooney, T.O., 2017, The Cenozoic magmatism of East-Africa: Part I — Flood basalts and pulsed magmatism:
794 Lithos, v. 286–287, p. 264–301, doi:10.1016/j.lithos.2017.05.014.
- 795 Sandwell, D.T., Müller, R.D., Smith, W.H.F., Garcia, E., and Francis, R., 2014, New global marine gravity
796 model from CryoSat-2 and Jason-1 reveals buried tectonic structure: Science, v. 346, p. 65–67,
797 doi:10.1126/SCIENCE.1258213.
- 798 Schettino, A., Macchiavelli, C., Pierantoni, P.P., Zaroni, D., and Rasul, N., 2016, Recent kinematics of the
799 tectonic plates surrounding the red sea and gulf of aden: Geophysical Journal International, v. 207,
800 p. 457–480, doi:10.1093/gji/ggw280.
- 801 Schettino, A., Macchiavelli, C., and Rasul, N.M.A., 2018, Plate motions around the red sea since the early
802 oligocene, in Geological Setting, Palaeoenvironment and Archaeology of the Red Sea, Springer
803 International Publishing, p. 203–220, doi:10.1007/978-3-319-99408-6_9.
- 804 Schult, A., 1974, Palaeomagnetism of tertiary volcanic rocks from the Ethiopian southern plateau and the
805 Danakil block: Journal of Geophysics, v. 40, p. 203–212,
806 <https://journal.geophysicsjournal.com/JofG/article/view/277> (accessed June 2021).
- 807 Sembroni, A., Faccenna, C., Becker, T.W., Molin, P., and Abebe, B., 2016, Long-term, deep-mantle support
808 of the Ethiopia-Yemen Plateau: Tectonics, v. 35, p. 469–488, doi:10.1002/2015TC004000.Received.
- 809 Sengör, A.M.C., and Burke, K., 1978, Relative timing of rifting and volcanism on Earth and its tectonic
810 implications: Geophysical Research Letters, v. 5, p. 419–421, doi:10.1029/GL005I006P00419.
- 811 Sobolev, S. V., Sobolev, A. V., Kuzmin, D. V., Krivolutsкая, N.A., Petrunin, A.G., Arndt, N.T., Radko, V.A.,
812 and Vasiliev, Y.R., 2011, Linking mantle plumes, large igneous provinces and environmental
813 catastrophes: Nature, v. 477, p. 312–316, doi:10.1038/nature10385.
- 814 Stockli, D.F., and Bosworth, W.B., 2018, Timing of extensional faulting along the magma-poor central and
815 northern red sea rift margin-transition from regional extension to necking along a hyperextended
816 rifted margin, in Geological Setting, Palaeoenvironment and Archaeology of the Red Sea, Springer
817 International Publishing, p. 81–111, doi:10.1007/978-3-319-99408-6_5.
- 818 Su, H., and Zhou, J., 2020, Timing of Arabia-Eurasia collision: Constraints from restoration of crustal-scale
819 cross-sections: Journal of Structural Geology, v. 135, p. 104041, doi:10.1016/j.jsg.2020.104041.
- 820 Szymanski, E., Stockli, D.F., Johnson, P.R., and Hager, C., 2016, Thermochronometric evidence for diffuse
821 extension and two-phase rifting within the Central Arabian Margin of the Red Sea Rift: Tectonics, v.
822 35, p. 2863–2895, doi:10.1002/2016TC004336.
- 823 Tazieff, H.T., Varet, J., Barberi, F., and Giglia, G., 1972, Tectonic significance of the Afar (or Danakil)
824 depression: Nature, v. 235, p. 144–147.
- 825 Tesfaye, S., Harding, D.J., and Kusky, T.M., 2003, Early continental breakup boundary and migration of the
826 Afar triple junction, Ethiopia: Bulletin of the Geological Society of America, v. 115, p. 1053–1067,
827 doi:10.1130/B25149.1.
- 828 Varet, J., 2018, Geology of Afar (East Africa): 1–249 p.
- 829 Varet, J., 1978, Geology of central and southern Afar (Ethiopia and Djibouti Republic): Paris, Centre
830 national de la recherche scientifique.

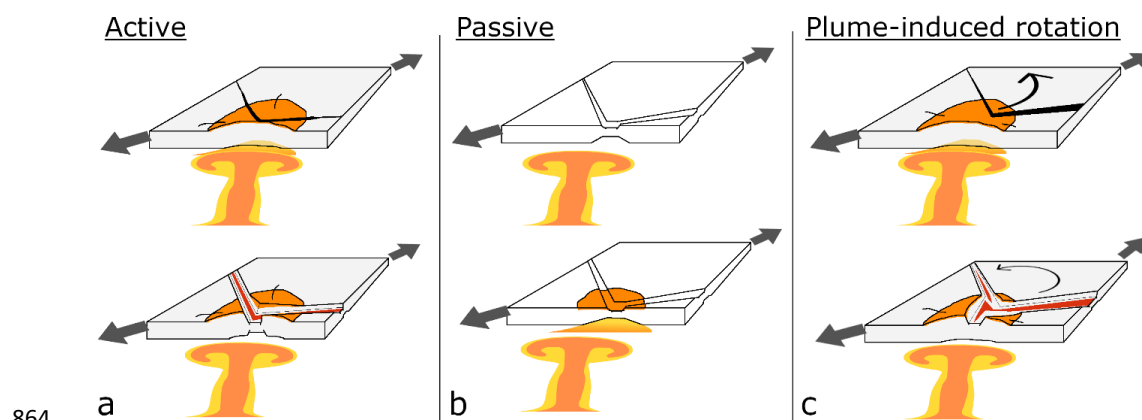


- 831 Viltres, R., Jónsson, S., Alothman, A.O., Liu, S., Leroy, S., Masson, F., Doubre, C., and Reilinger, R., 2022,
832 Present-Day Motion of the Arabian Plate: Tectonics, v. 41, p. e2021TC007013,
833 doi:https://doi.org/10.1029/2021TC007013.
- 834 Viltres, R., Jónsson, S., Ruch, J., Doubre, C., Reilinger, R., Floyd, M., and Ogubazghi, G., 2020, Kinematics
835 and deformation of the southern Red Sea region from GPS observations: Geophysical Journal
836 International, v. 221, p. 2143–2154, doi:10.1093/gji/ggaa109.
- 837 Watchorn, F., Nichols, G.J., and Bosence, D.W.J., 1998, Rift-related sedimentation and stratigraphy,
838 southern Yemen (Gulf of Aden), *in* Sedimentation and Tectonics in Rift Basins Red Sea:- Gulf of Aden,
839 Springer Netherlands, p. 165–189, doi:10.1007/978-94-011-4930-3_11.
- 840 Wescott, W.A., Wigger, S.T., Stone, D.M., and Morley, C.K., 1999, AAPG Studies in Geology# 44, Chapter 3:
841 Geology and Geophysics of the Lotikipi Plain:
- 842 White, R., and McKenzie, D., 1989, Magmatism at rift zones: the generation of volcanic continental margins
843 and flood basalts: Journal of Geophysical Research, v. 94, p. 7685–7729,
844 doi:10.1029/JB094iB06p07685.
- 845 White, R.S., and McKenzie, D., 1995, Mantle plumes and flood basalts: Journal of Geophysical Research, v.
846 100, p. 543–560, doi:10.1029/95jb01585.
- 847 Will, T.M., and Frimmel, H.E., 2018, Where does a continent prefer to break up? Some lessons from the
848 South Atlantic margins: Gondwana Research, v. 53, p. 9–19, doi:10.1016/j.gr.2017.04.014.
- 849 Wilson, J.T., 1963, A possible origin of the Hawaiian Islands: Canadian Journal of Physics, v. 41, p. 863–870,
850 doi:10.1139/P63-094.
- 851 Wolfenden, E., Ebinger, C., Yirgu, G., Deino, A., and Ayalew, D., 2004, Evolution of the northern Main
852 Ethiopian rift: Birth of a triple junction: Earth and Planetary Science Letters, v. 224, p. 213–228,
853 doi:10.1016/j.epsl.2004.04.022.
- 854 Zingerle, P., Pail, R., Gruber, T., and Oikonomidou, X., 2020, The combined global gravity field model
855 XGM2019e: Journal of Geodesy 2020 94:7, v. 94, p. 1–12, doi:10.1007/S00190-020-01398-0.
- 856 Zwaan, F., Corti, G., Keir, D., and Sanj, F., 2020, A review of tectonic models for the rifted margin of Afar:
857 Implications for continental break-up and passive margin formation: Journal of African Earth
858 Sciences, v. 164, doi:10.1016/j.jafrearsci.2019.103649.



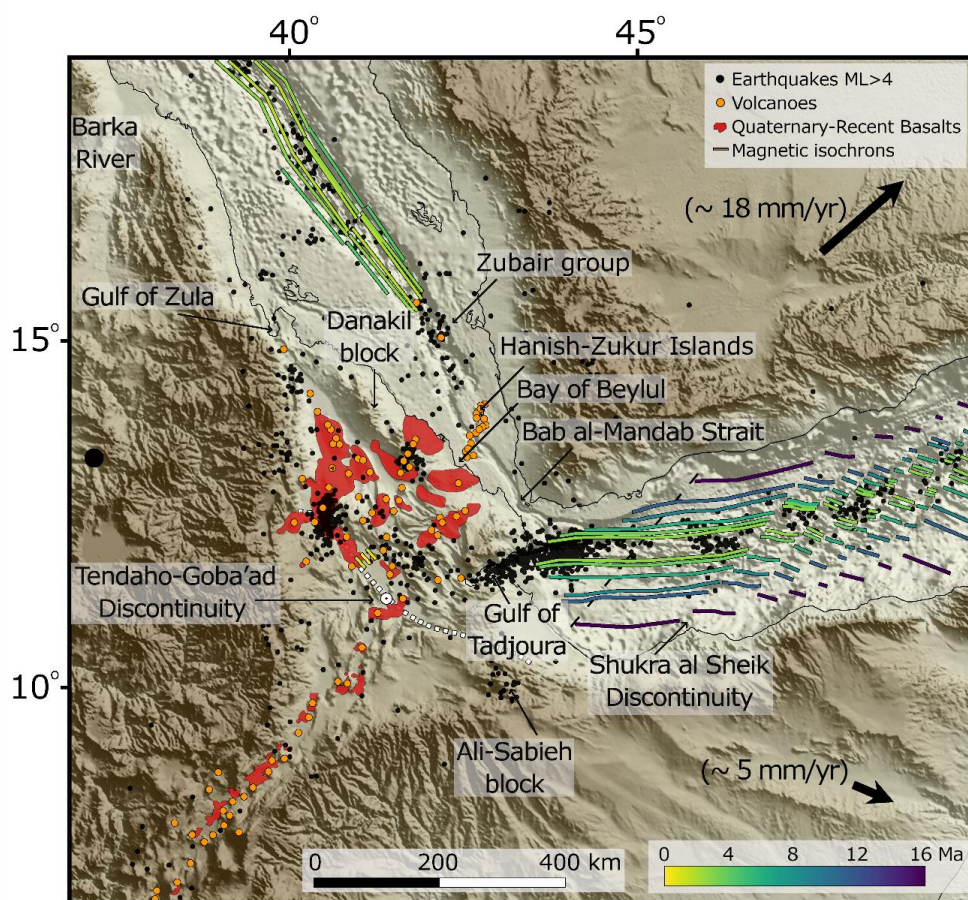
859

860 **Figure 1.** Elevation map of the study area, showing the general plate tectonic configuration (from USGS
861 and from Viltres et al., (2020) in the Afar region) and Cenozoic volcanics (modified from Varet, 1978;
862 Davison et al., 1994; Beyene and Abdelsalam, 2005; Bosworth and Stockli, 2016) Black arrows indicate GPS
863 velocities in respect to Nubia (modified from Reilinger et al., 2006).



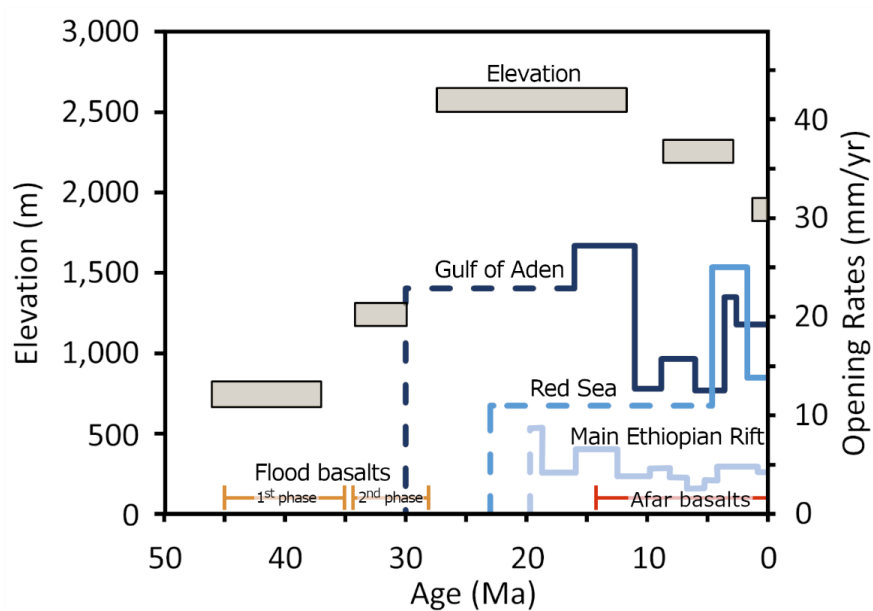
864

865 **Figure 2.** Schematic mechanisms for plume-rift association in the Afro-Arabian rift. (a) Active mechanism,
866 in which rifting results from the actively rising head of the Afar plume. In this mechanism impinging and
867 eroding the base of the lithosphere prompt uplift and decompression melting and flood basalts volcanism.
868 These introduce internal extensional forces and ultimately lead to break-up. (b) Passive mechanism, in
869 which rifting is initiated solely by the remote stresses, regardless of underlying Afar plume. In this
870 mechanism the production of massive volcanism is allowed when the thinned and stretched lithosphere
871 is underlaid by the thermal anomaly in the mantle. Flood basalts volcanism is generated by passively rising
872 decompression melting of hot asthenospheric mantle. (c) Plume-induced plate rotation, in which lateral
873 forces, induced by the arrival of the Afar plume head, add up to the remote stresses to change the plate
874 kinematics. In this mechanism flood basalts volcanism is actively controlled, however, rifting is triggered
875 by the new plate kinematics.



876

877 **Figure 3.** Map of the Afar region showing magnetic isochrons (modified from Fournier et al., 2010; Bridges
878 et al., 2012; Schettino et al., 2016), earthquake locations (from ISC catalog), Holocene onshore volcano
879 locations (from GVP catalog and Viltres et al., (2020)) and recent volcanism (modified from Keir et al.,
880 2013).



881

882 **Figure 4.** Elevation of the Ethiopian–Yemen plateau (after Sembroni et al., 2016; Faccenna et al., 2019),
883 volcanic episodes and opening rates of the rift arms (modified from Fournier et al., 2010; DeMets and
884 Merkouriev, 2016; Schettino et al., 2018). Dashed lines indicate estimations from geological observations
885 and solid lines from magnetic isochrons.

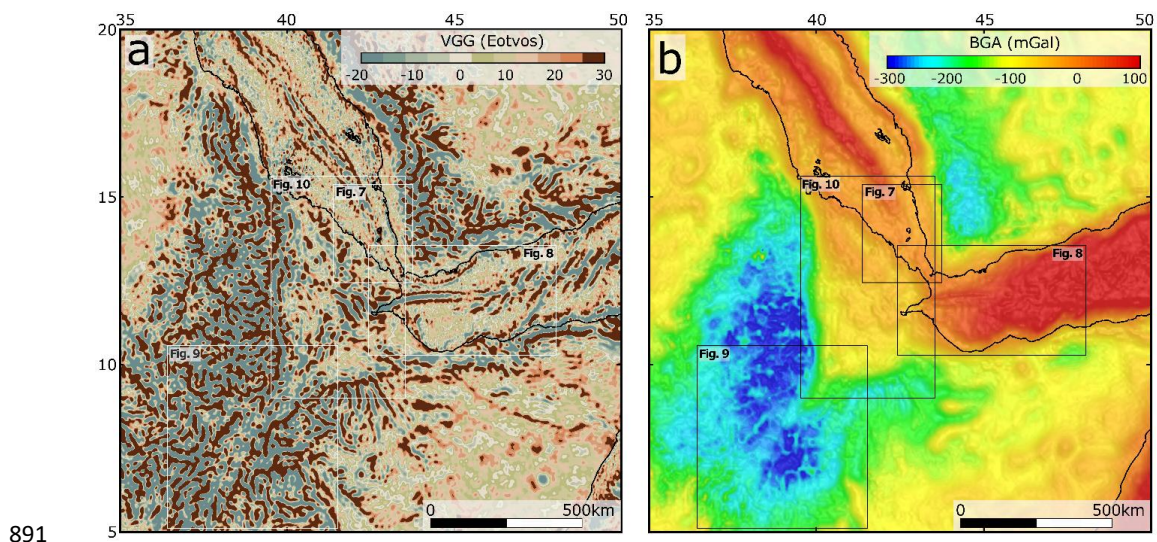
886

887

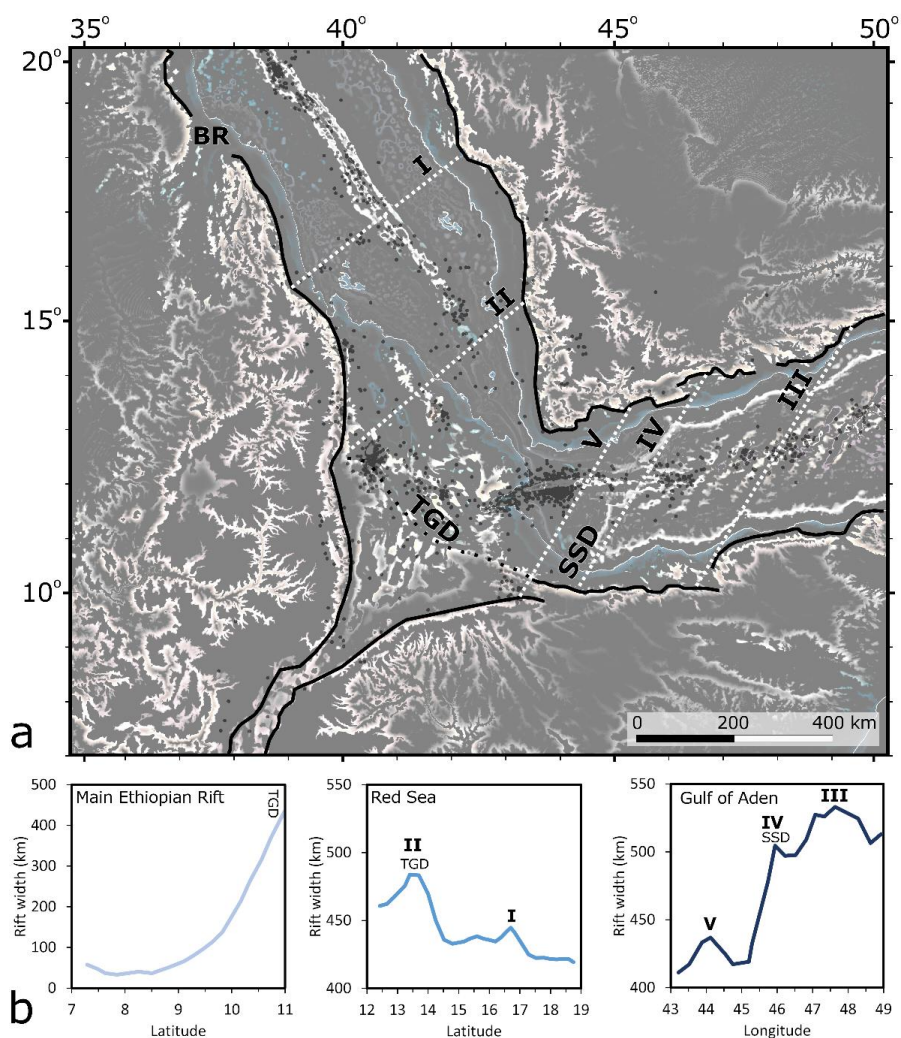
888

889

890

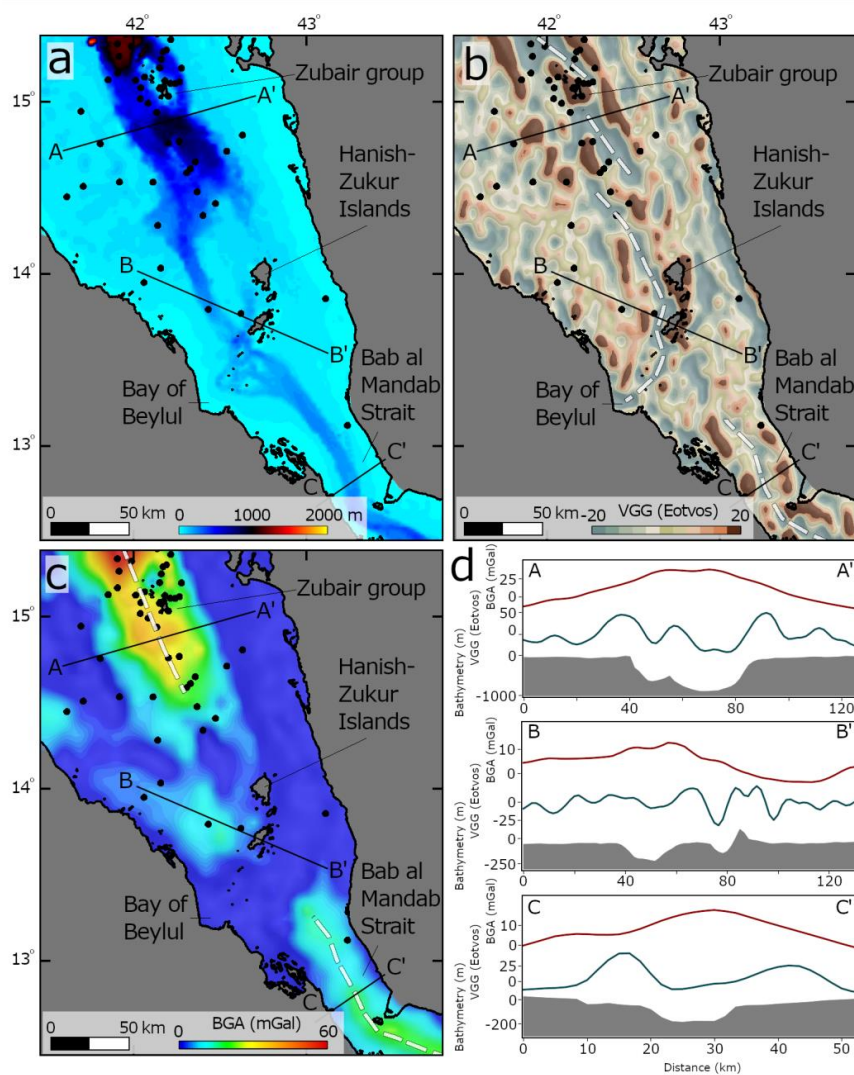


892 **Figure 5.** Gravity data of the Afar region. (a) Vertical gravity gradient from Sandwell et al. (2014). Bouguer
893 anomaly model from ICGEM, XGM2019e (Zingerle et al., 2020).



894

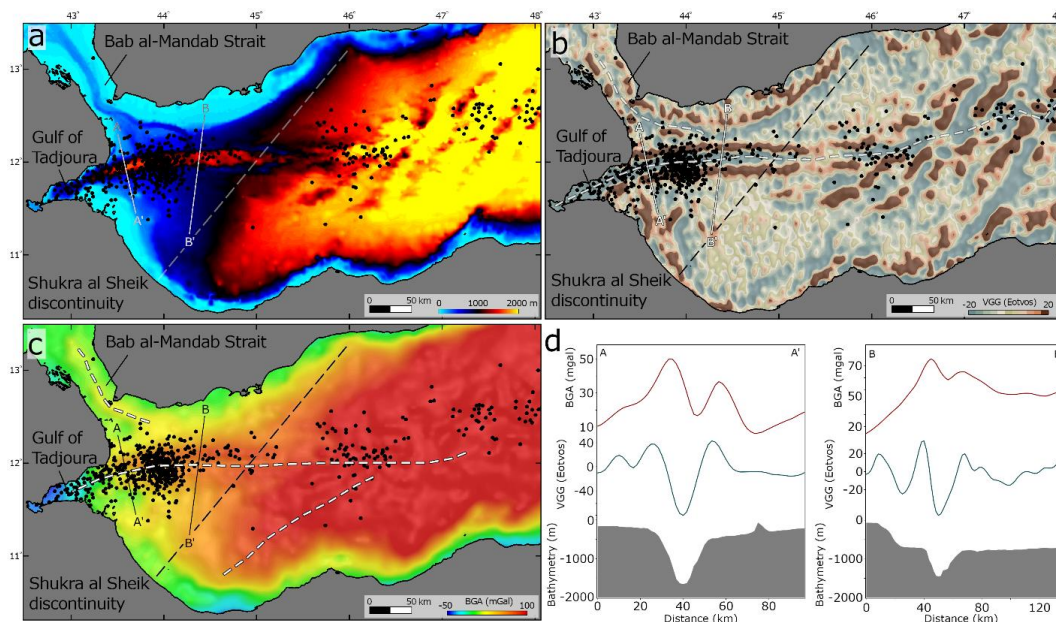
895 **Figure 6.** (a) Difference of Gaussians applied to topography and bathymetry showing rift margins (black
896 lines). White dashed lines indicate peaks in rift width. TGD is the Tendaho-Goba'ad Discontinuity. SSD is
897 the Shukra al Sheik discontinuity. Black dots indicate earthquake locations (ISC catalog). (b) Rift widths,
898 calculated in rift-perpendicular directions.



899

900 **Figure 7.** Bathymetry (a), vertical gravity gradient (b) and Bouguer anomaly (c) in the southern Red Sea.

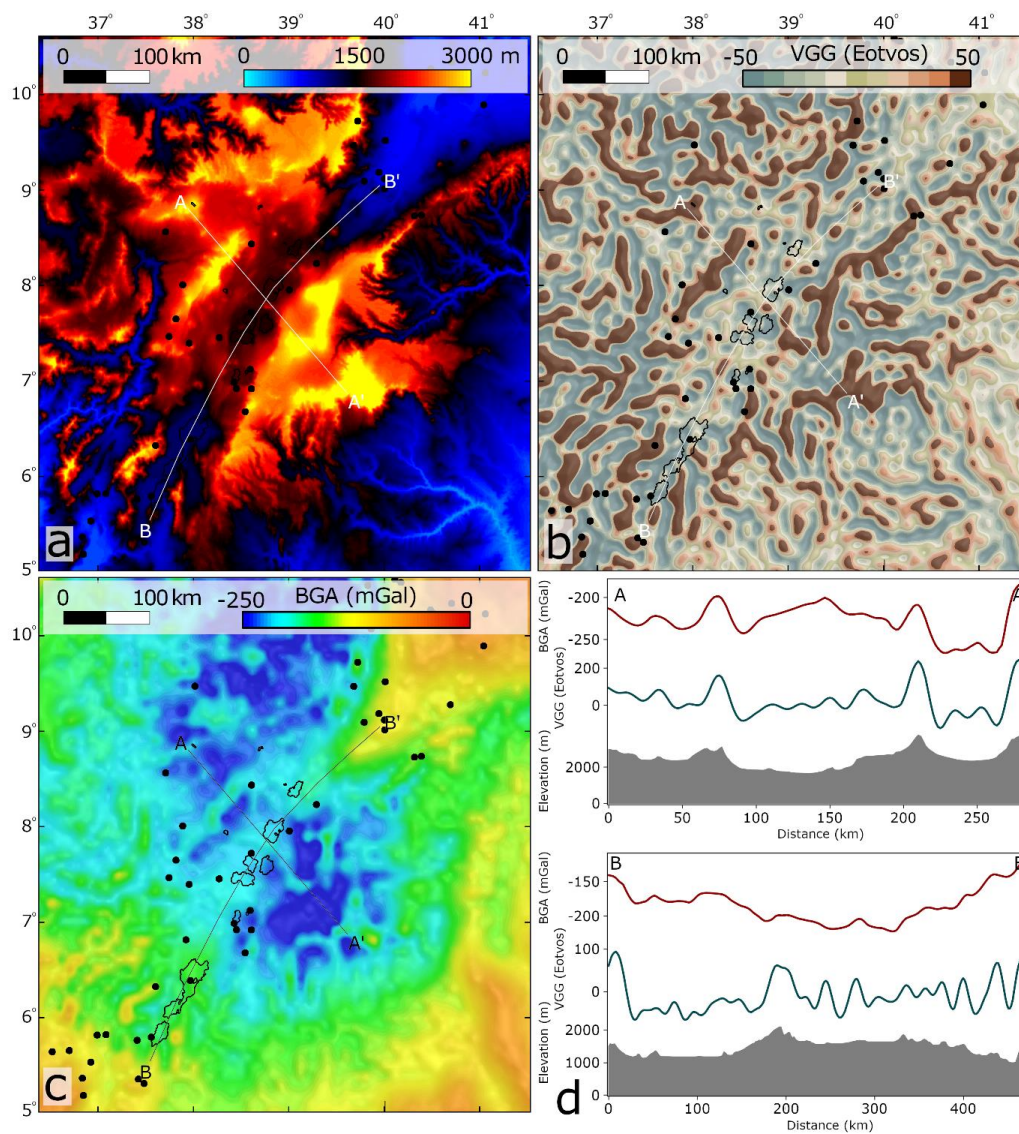
901 Black dots indicate earthquake locations (ISC catalog). (d) Profiles across rift axis.



902

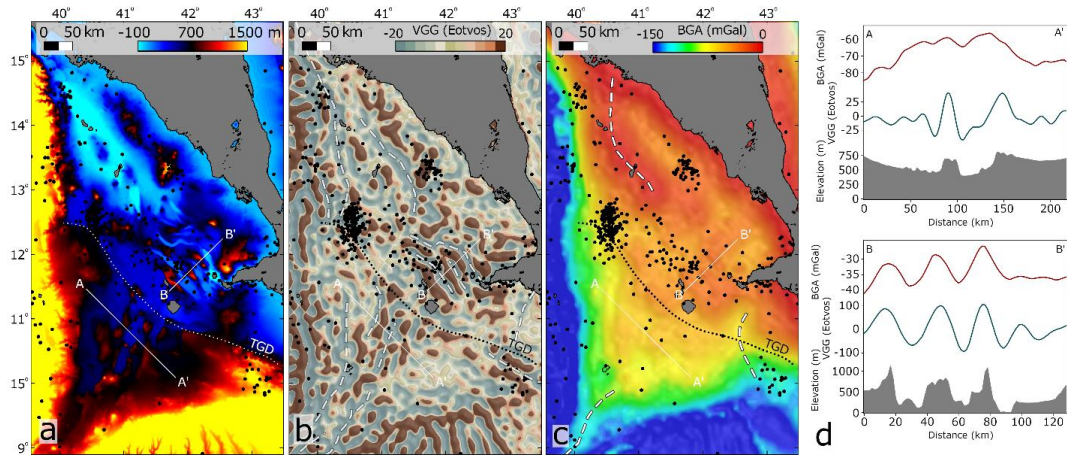
903 **Figure 8.** Bathymetry (a), vertical gravity gradient (b) and Bouguer anomaly (c) in the Western Gulf of Aden.

904 Black dots indicate earthquake locations (ISC catalog). (d) Profiles across rift axis.



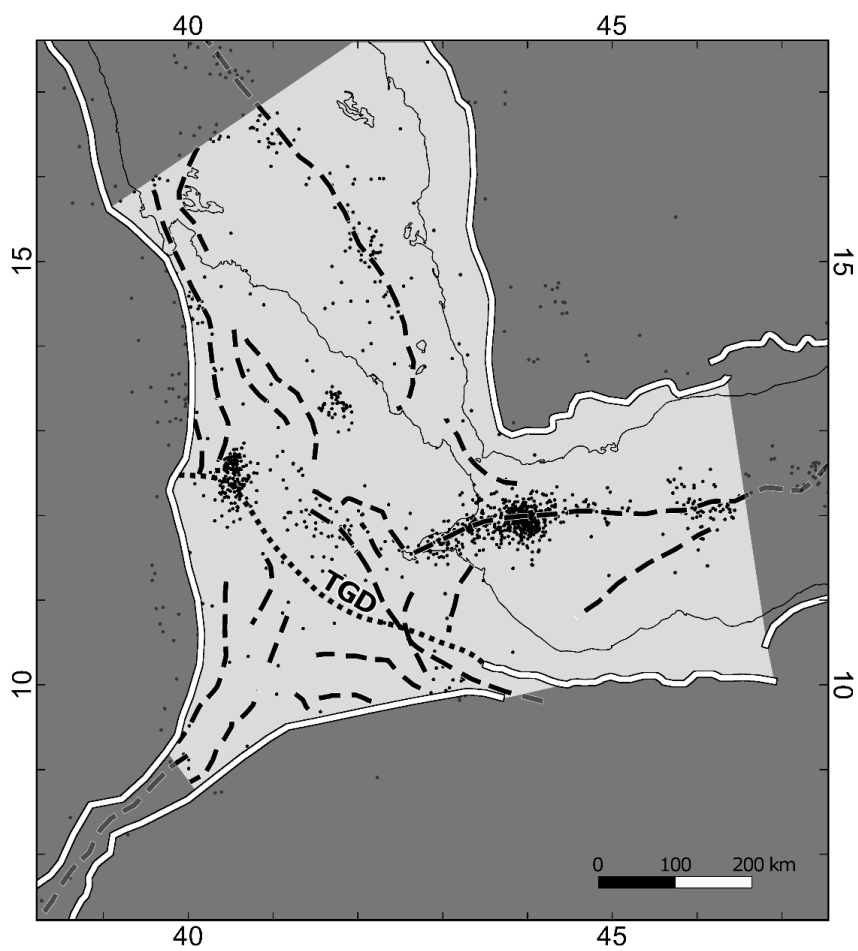
905

906 **Figure 9.** Topography (a), vertical gravity gradient (b) and Bouguer anomaly (c) in the northern Main
907 Ethiopian Rift. Black dots indicate earthquake locations (ISC catalog). (d) Profiles across (AA') and along
908 (BB') the rift valley.



909

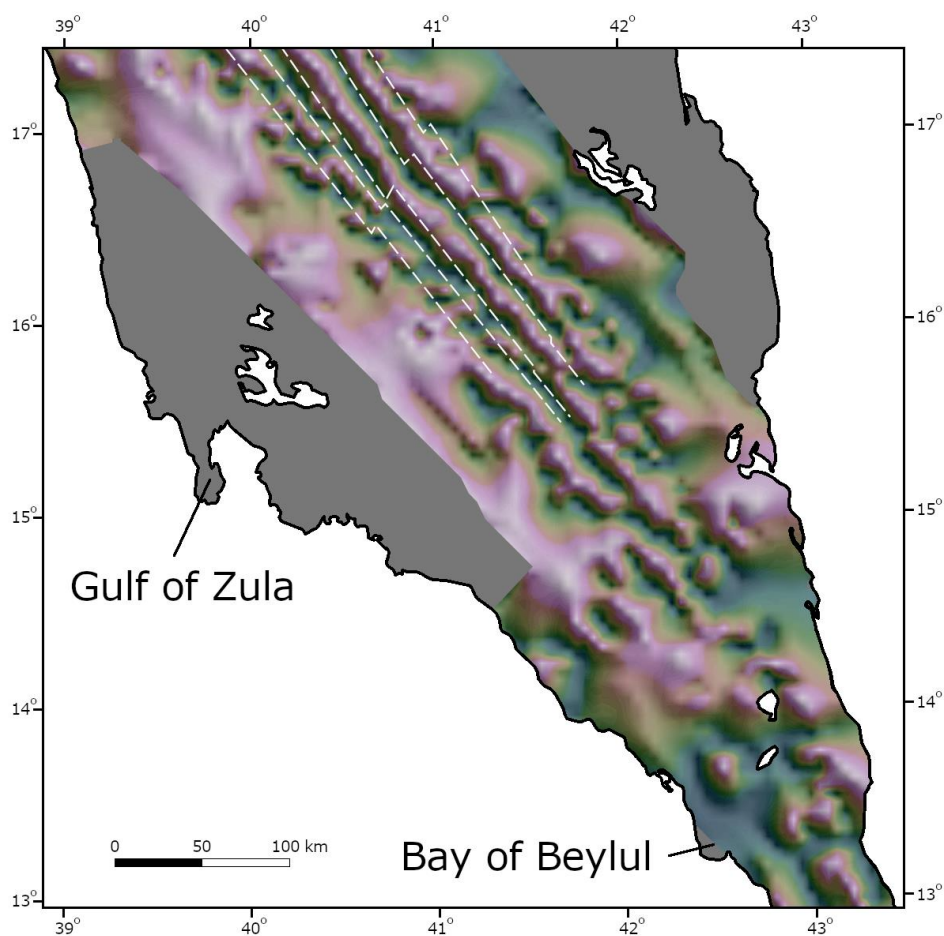
910 **Figure 10.** Topography (a), vertical gravity gradient (b) and Bouguer anomaly (c) in the Afar triangle. Black
911 dots indicate earthquake locations (ISC catalog). TGD is the Tendaho-Goba'ad Discontinuity. (d) Profiles
912 SW (AA') and NE (BB') to the TGD.



913

914 **Figure 11.** Rift margins (solid white lines) and axial segments (long dashed black lines) in the Afar region.

915 Black dots indicate earthquake locations (ISC catalog). TGD is the Tendaho-Goba'ad Discontinuity.



916

917 **Figure 12.** Tilt-angle derivative map of magnetic anomalies, projected on a shaded relief after Issachar et
918 al. (2022). Purple colours represent positive angles and green colors represent negative angles. White
919 dashed lines indicate magnetic stripes (Schettino et al., 2016).

920

921

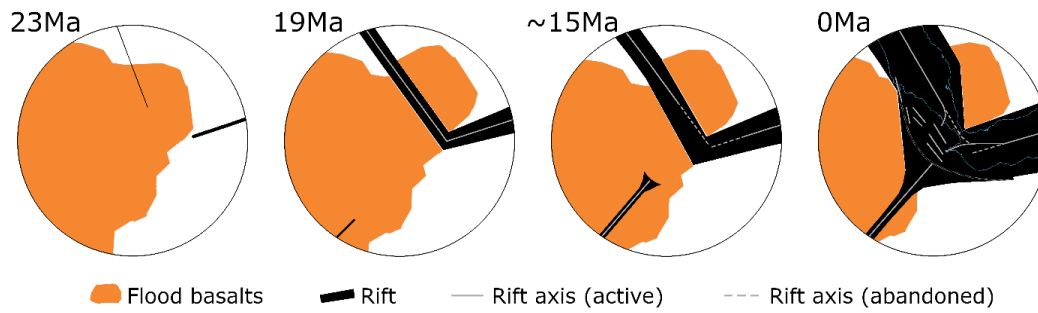
922

923

924

925

926



927

928 **Figure 13.** Synthesis of the progressive development of the rift intersections.